RC25045 (W1009-018) September 14, 2010
Materials Science

IBM Research Report

Effects of Minor Alloying Additions on the Properties and Reliability of Pb-free Solders and Joints

Sung K. Kang
IBM Research Division
Thomas J. Watson Research Center
P.O. Box 218
Yorktown Heights, NY 10598

Research Division
Almaden - Austin - Beijing - Cambridge - Haifa - India - T. J. Watson - Tokyo - Zurich

LIMITED DISTRIBUTION NOTICE: This report has been submitted for publication outside of IBM and will probably be copyrighted if accepted for publication. It has been issued as a Research Report for early dissemination of its contents. In view of the transfer of copyright to the outside publisher, its distribution outside of IBM prior to publication should be limited to peer communications and specific requests. After outside publication, requests should be filled only by reprints or legally obtained copies of the article (e.g., payment of royalties). Copies may be requested from IBM T. J. Watson Research Center , P. O. Box 218, Yorktown Heights, NY 10598 USA (email: reports@us.ibm.com). Some reports are available on the internet at http://domino.watson.ibm.com/library/CyberDig.nsf/home .

"Effects of Minor Alloying Additions on the Properties and Reliability of Pb-free Solders and Joints"

Sung K. Kang

IBM T.J. Watson Research Center, Yorktown Heights, NY 10598, USA

(Tel) 914-945-3932, (email) kang@us.ibm.com

Abstract

Since July, 2006, following the EU's RoHS legislation, the consumer electronics industry has been offering "green" products by eliminating Pb-containing solders and other toxic materials. This transition has been relatively smooth, because the reliability requirements are less stringent. However, the Pb-free transition for high performance electronic systems (such as servers and telecommunication) is still on-going due to their rigorous reliability requirements. For example, the research and development efforts to implement Pb-free flip chip interconnections for high end applications are still very active.

In this paper, the recent progress in Pb-free solder development, especially minor alloy additions to Sn-rich solders is reviewed in light of improving various physical, mechanical, metallurgical or electrical properties of solder joints. The topics to be discussed include such as control of undercooling, microstructure, interfacial reactions, or void formation, as well as enhancing impact resistance, electromigration, and other mechanical properties.

1. Introduction

Extensive searches for Pb-free solders have been conducted in 1990's to find an ideal "drop-in" replacement of eutectic Pb/Sn solder predominantly used in microelectronic applications [1-9]. However, such a replacement was not found. Instead, several promising candidates of Sn-rich solders were identified for different soldering applications as listed in Table I. Among them, binary eutectic solders, Sn-Cu or Sn-Ag, and ternary Sn-Ag-Cu or Sn-Ag-Bi were recommended for major soldering applications, such as SMT card assembly [3-7].

When the European Union passed the RoHS (Restriction of Hazardous Substances) directive in October 2002, banning several toxic materials including Pb in electrical and electronic systems from July 1, 2006, the R&D activities on Pb-free solders became more intensified. By the early 2000's, the near-ternary eutectic Sn-Ag-Cu (SAC) alloy compositions of melting temperatures around 217ºC became a consensus candidate in US as well as abroad [10-18]. Some variations of SAC solders are included in Table 1. In general, low-Ag SAC compositions were adopted in Japan, while high-Ag versions were preferred initially in US.

Subsequently, extensive research and development efforts have been focused on the Sn-Ag-Cu system to evaluate the reliability risk factors associated with SAC solder joints, compared to the well established Pb-containing solder joints [19-29].

Recently, many new findings on fundamental issues of Sn-rich solders have been reported, especially on Sn-Ag-Cu system. A few examples are listed here, such as severe interfacial reactions during reflow or thermal aging [6, 19], large Ag_3Sn plate formation [14], large undercooling during Sn solidification [17,18], unique twining microstructure in Sn-Ag or Sn-Ag-Cu [28], anisotropic physical/mechanical properties of Sn crystals [28], fast diffusions of Cu, Ag and Ni solute atoms along the c-axis of β-Sn crystal [30-32], only a few grains in BGA or flip chip joints [15] and others. These new findings have also closely related with the reliability issues of Sn-rich solder joints. To name a few items, such as excessive Cu consumption [26], easy fatigue crack growth along large Ag_3Sn plates [16], chip joining issues due to large undercooling [33], void formation and drop impact failure [22-24], crystal orientation effects on thermal fatigue [28] and electromigration [34], and others.

In an effort to mitigate the reliability risk factors associated with Sn-Ag-Cu joints, the world-wide research community on Pb-free solders has lately directed their efforts on modifying the compositions of the SAC solders by adding minor alloying elements.

In this paper, some of the new findings and their impacts on the reliability and integrity of Pb-free solder joints are discussed in order to reduce the reliability risk factors in implementing Pb-free solder technology.

It is remarkable to note that numerous alloy modifications of Sn-rich solders have already been well documented in the patent literature on Pb-free solders for the past 20 years or so. Table II, III, and IV collect about 100 US patents on Pb-free solders, mostly with Sn-rich compositions and a few Bi-rich compositions. Tables also show the composition ranges of various alloying elements, such as Ag, Bi, Cu, In, Ni, Sb, Zn and others. Since this patent literature covers a wide range of minor alloying elements added to Sn-rich solders, it would be very useful to the following discussion.

2. Controlling Ag_3Sn Plate Formation

The microstructure of ternary eutectic Sn-Ag-Cu solder consists of three different phases β-Sn (m.p., 232^oC), Cu_6Sn_5 (415^oC), and Ag_3Sn (480^oC), with the ternary eutectic temperature, about 217^oC [10]. Fig. 1 shows a typical microstructure of near-ternary SAC formed at a relatively slow cooling rate. The β-Sn dendrite cells were surrounded by the ternary eutectic regions which are a mixture of fine intermetallic particles of Cu_6Sn_5 and Ag_3Sn in the β-Sn matrix. This microstructure suggests that Sn dendrites solidified first and then immediately followed by the eutectic solidification. In the middle of Fig.1, a large plate-like Ag_3Sn phase grown across the Sn dendrite cells is noted. This large Ag_3Sn plate is a proeutectic phase of an intermetallic compound (IMC), nucleated well above the ternary eutectic temperature and continued to grow in the liquid solder until the solidification process ends. The presence of the large Ag_3Sn plate indicates that the overall solidification process was not under equilibrium and its microstructure must be off the ternary eutectic as shown. From the microhardness test on each phase, it was confirmed that the large Ag_3Sn plate has a considerably higher hardness (HVN ~126.5) than the Sn dendrite matrix (HVN; 15.2 to 26.5) [35]. This suggests the formation of large Ag_3Sn plate being regarded as not desirable in view of their microstructure and mechanical properties of SAC joints.

Fig. 2 shows an example of a large Ag_3Sn plate adversely affected the fatigue life of a CBGA (ceramic ball grid array) package [13]. Due to the strain localization at the boundary between the Ag_3Sn plates and the bounding β-Sn phase, the interface provided a preferential crack propagation path, leading to a premature failure during the thermal cycling testing. To improve

thermal fatigue life of near-ternary SAC joints, it is desirable to suppress the formation of large Ag_3Sn plates.

A systematic study on the formation of large Ag_3Sn plate in near-ternary SAC solder and joints was conducted in terms of cooling rate, Ag and Cu content [35, 36]. The cooling rate was found to be a crucial factor in forming large Ag_3Sn plates. At a high cooling rate, there would be not enough time for Ag_3Sn plates to grow into a large size, if even they were nucleated. This is consistent with the observation that large Ag_3Sn plates are not commonly observed in solder joints rapidly cooled at a rate of $1^oC/s$ or higher. Hence, the formations of large Ag_3Sn plates can be *kinetically* controlled by employing a high cooling rate, such as $1.5^oC/s$ or higher during a reflow process. However, providing a high cooling rate is not always practical, especially, with a substrate of a large thermal mass because of unwanted high thermal stress or strain induced. In the same study, complete dissolution of large Ag_3Sn plates (about 500 micron long) was demonstrated after 3 min reflow at 250 °C [35]. However, in a conventional reflow large Ag_3Sn plates would not dissolve completely due to a limited time provided above the liquidus temperature, and the remaining Ag_3Sn plates can grow back quickly to a large size in a subsequent cooling step.

To investigate the effect of Ag content, several SAC solders with reduced Ag contents were evaluated from 2.0 to 3.8% with a fixed Cu content. Table 5 lists the melting point and the amount of undercooling measured with these SAC alloys. The melting point of SAC solders is not sensitive to Ag content, while the amount of the undercooling varied from 18 to 34^oC. A strong correlation between the Ag content and the population of large Ag_3Sn plates (larger than 100 micron long) was observed in this study. Solder balls were heated to 250^oC, held there for 10 min, and then cooled slowly at a rate of $0.02^oC/s$ to room temperature. The microstructure of about 100 solder balls from each group was examined to count the number of solder balls containing at least one large Ag_3Sn plate of 100μm or longer. The frequency of observation of large Ag_3Sn plates is summarized in Table 6. For the SAC alloy with 3.8 % Ag, 76 out of 100 balls contained large Ag_3Sn plates, while almost no balls contained large Ag_3Sn plates in the slow-cooled solders with the Ag content less than 3.0 wt %. Large Ag_3Sn plates were substantially reduced in the SAC alloys of less than 3 wt % Ag, even in an extremely slow-cooled condition, such as $0.02^oC/s$. Hence, the formation of large Ag_3Sn plates can be *thermodynamically* suppressed by lowering the Ag content below 3 wt %. This dependence on Ag content was further explained by a

thermodynamic calculation using an isopleth phase diagram of Sn-XAg-0.7Cu [35]. The Ag_3Sn liquidus was determined in the metastable region by directly extrapolating the liquidus from the ternary eutectic temperature. As listed in Table 5, the solidification process in the Sn-3.8Ag-0.7Cu alloy requires an undercooling of 15 to 30^oC before the Sn phase solidifies. The metastability of the liquid Sn phase would depend on the available sites for heterogeneous nucleation to take place. At a nominal Cu concentration of 0.7 % in the liquid, the composition of the liquidus intersecting at 20^oC undercooling is approximately 2.7 wt % Ag. Thus, for compositions equal to or less than 2.7 wt % Ag, the Ag_3Sn phase would be difficult to nucleate or grow within the liquid in a solder joint without undercooling in excess of 20^oC.

The effect of Cu content on large Ag_3Sn plate formation was somewhat different from Ag content. Many large Ag_3Sn plates were found in slowly-cooled ingots of Sn-3.8Ag-0.35Cu and Sn-3.8Ag-0.7Cu, but much less in Sn-3.5Ag [35].The presence of Cu in the solder appears to promote the formation of large Ag_3Sn plates, but it is not explicitly clear how this effect occurs. One possible explanation was provided by noting that more Cu atoms were measured in a large Ag_3Sn plate (about 0.36 wt % Cu) than in β-Sn dendrites (about 0.16 wt % Cu), [10]. Hence, the role of Cu atoms in nucleating a large Ag_3Sn plate, not in growth, was suggested. Since only a small amount of Cu atoms may need to nucleate an Ag_3Sn plate in an undercooled SAC alloy, this may explain why no difference in the population of large Ag_3Sn plates was observed for a different Cu composition, such as 0.35 vs 0.7 wt %.

Another method of controlling the formation of large Ag_3Sn plates was reported by adding a small amount of Zn to the near-ternary SAC solders [14]. As discussed in the following section, the Zn addition into SAC (such as 0.1 wt %) is very effective to reduce the undercooling required for β–Sn solidification and thereby to suppress the formation of large Ag_3Sn plates even at a very slow cooling rate (such as 0.02°C/s). The Zn addition did coarsen Sn dendrites and increase the volume fraction of the eutectic regions. It was also reported that a preferential reaction between Zn and Cu atoms occurred in the solder matrix as well as at the interface of Cu metallization. To control the formation of large Ag_3Sn plates, the Zn addition in the range from 0.1 to 0.7 wt % was recommended, depending on its metallization or solder volume [14].

The presence of large Ag_3Sn plates in small solder joints such as flip-chip solder bumps can be a serious issue of affecting the joint integrity and reliability. Fig. 3 shows an example of a

flip-chip joint made of Sn-3.8Ag-0.7Cu solder reflowed twice at 260°C on a Cu substrate [19]. The large plate-like Ag_3Sn IMCs extended to a substantial distance in a small flip chip joint after reflow, while relatively small Cu_6Sn_5 IMCs were mostly attached to the interface. The microstructure and mechanical properties of this joint would be seriously altered by the large IMCs, and consequently the reliability of the joint would be affected.

Another interesting example of large Ag_3Sn plates was reported with electroplated Sn-Ag solder bumps fabricated by a wafer bumping process for flip-chip applications, as shown in Fig. 4 [37]. Large Ag_3Sn plates or needles were precipitated on top of solder bumps after multiple reflows. Some of large Ag_3Sn plates were even shorting neighboring bumps. To avoid this undesirable situation, the Ag content of electroplated Sn-Ag bumps was reduced below 2.7 wt % , following the recommendations provided by the previous works [13, 35, 36]. Since then, the low Ag content in electroplated Sn-Ag bumps has been adopted for Pb-free flip-chip wafer bumping applications.

3. Controlling the Undercooling of Sn Solidification

The undercooling is defined as the temperature difference between the melting temperature of a solder during heating and the solidification temperature during cooling. A typical DSC (differential scanning calorimetry) thermal profile recorded during the heating and cooling cycle of one solder ball of Sn-0.9%Cu (50-mil diameter) is shown in Fig. 5. The onset and peak temperatures during heating are 228.6°C and 230.5°C, respectively, and those during cooling are 199.7°C (onset) and 202.0°C (peak). The undercooling is then estimated to be about 28-29°C depending on either the onset or peak temperatures [29]. Table 7 reports the amount of the undercooling measured with several Pb-free solders. The undercooling of Sn-rich solders, namely, Sn-Cu, Sn-Ag and Sn-Ag-Cu, is not significantly affected by varying Cu or Ag content or both. This suggests that Cu and Ag solute atoms themselves or their intermetallic compounds, such as Cu_6Sn_5 or Ag_3Sn, may not provide preferential nucleation sites for β–Sn solidification. However, the addition of a small amount of Co, Fe, or Zn is found to be very effective to reduce the undercooling by more than 20°C as listed in Table 7.

The undercooling required for solidification of near-ternary Sn-Ag-Cu solders is generally much larger than high Pb solders or Sn-Pb eutectic solders [17, 35]. This large undercooling is

also responsible for the growth of large primary phases of Ag_3Sn or Cu_6Sn_5 as shown in Fig. 1. It is also known that the undercooling amount in Sn-Ag-Cu solders is inversely proportional to sample size, suggesting a larger undercooling in a smaller solder joint (such as flip chip vs. BGA solder joints) [38]. A large undercooling and random solidification among flip-chip solder bumps can adversely affect the reliability of solder joints, since this would yield a situation of some bumps already solidified while others not, causing stress concentration to certain bumps and possibly leading to mechanical or electrical fails within solder joints or other weak structures within the package or in a Si device.

Controlling the undercooling of Sn-rich solders is an important issue in such a new wafer bumping process, C4NP (C4 New Process), where melting/solidification of multiple solder bumps in a small volume is a key metallurgical process involved [33, 39]. In C4NP, a molten solder is filled into a glass mold containing prefabricated cavities of I/O footprint of a silicon wafer, and then solder bumps are transferred from the glass mold to the wafer by aligning/melting the solidified bumps.

To understand the critical factors affecting the undercooling of Pb-free, flip-chip solder bumps in the C4NP process, a systematic investigation was conducted in terms of solder composition, solder volume, minor alloying elements, UBM (under bump metallization), cooling rate, impurity level, and others [29]. The undercooling of Pb-free, flip-chip solder bumps was evaluated by DSC and the direct observation of individual solder bumps in a glass mold during melting and solidification [29, 40]. The amount of the undercooling of Sn-rich solders was confirmed to be strongly affected by solder volume, inversely proportional to its volume (or effective diameter of solder balls). It was also found that the solder composition and UBM significantly affected the undercooling, but the cooling rate and holding temperature of the mold plate used in C4NP did not so much. Sn-0.7Cu C4NP solder bumps in a mold plate were undercooled by as much as 90°C from its melting point, while a less amount of undercooling (40 to 60°C) was observed on a Si chip having a wettable Cu/Ni UBM [29].

The effects of UBM on the undercooling were evaluated by comparing various Cu vs. Ni metallization, which included electroplated Cu, electroplated Ni, electroless Ni(P), electroless Ni(P)/immersion Au [41, 42]. The Ni-based UBM was found to be more effective than Cu UBM in reducing the undercooling of Pb-free solders investigated. To explain, the superior behavior of Ni over Cu UBM, both minor Cu- and Ni-doped solders were evaluated for their undercooling

behaviors [42]. It was concluded that the type of interfacial IMC phases (Cu_6Sn_5 vs. Ni_3Sn_4) was not the primary contributing factor, but the Ni atoms dissolved from Ni UBM and concurrent precipitation of Ni_3Sn_4 particles inside the solder matrix.

The direct observation of individual flip-chip-size solder bumps on a glass mold during their solidification process revealed the random nature of the molten solder nucleation process, and also confirmed the similar amount of the undercooling as measured by DSC [29, 40]. As the solder volume continuously decreases in the future flip-chip interconnect technologies, minimizing the undercooling of molten solders like in C4NP would become a more critical issue for reliable solder joints.

Since the undercooling phenomenon is related to the difficulty of nucleating a solid phase in a liquid solder, many studies have been reported by adding minor alloying elements into Sn or Sn-rich solders in order to provide some preferential nucleation sites. These minor alloying elements reported include such as Al, Be, Bi, Co, Fe, Hf, Mg, Mn, Mo, Ni, Pt, Ti, Zn, Zr, W, and others [9, 12, 14, 18, 25, 26, 35, 41-45]. Among them, Zn has been extensively investigated, because it is most effective and practical to be used with Sn or alloys [14, 25, 26, 43, 44].

In order to address why Zn or Co addition is so effective in reducing the undercooling, a variety of minor alloying elements to Sn-rich solders has been investigated in terms of their crystal structure [43]. Table 8 summarizes the amounts of the undercooling measured by DSC with several different crystal structures of the minor alloying elements. The content of the minor alloying elements is 0.2 wt % in all cases. It is quite interesting to note that the hexagonal crystal structure (HCP) of minor alloying elements is very effective in reducing the undercooling of pure Sn compared to other crystal structure groups. The minor additions of Zn and Ti of the hexagonal crystal structure are again confirmed to be most effective among others. Subsequently, several other HCP metals, such as Co, Mg, Sc and Zr, were evaluated to verify their effectiveness. Table 9 summarizes the results of the undercooling measurement with all the HCP metals investigated. Indeed, the minor alloying elements of HCP crystal structure are confirmed to be very effective in reducing the undercooling of the pure Sn down to about $6^{o}C$ or less. The Zn addition is again shown to be most effective among all other HCP metals.

In his Ph.D. thesis, M. G. Cho has further explained why the hexagonal metals, especially Zn is most effective by comparing the lattice coherency between Pb/β-Sn and Zn/β-Sn, finding an excellent matching surface, (10-11) of Zn to the β-Sn lattice, while not possible with the Pb structure. This matching surface is suggested to act as a more favorable nucleation site for the Sn nucleation. In addition, employing DFT (density function theory) calculation, it has shown that the interfacial energy between β-Sn and Zn is relatively low, and especially the lowest on the (10-11) surface of Zn [46].

4. Controlling Interfacial Reactions

The interfacial reactions with UBM (Under Bump Metallization) or surface finishes of solder joints start during a joining/rework process and continue in testing or field service of electronic packages. Proper interfacial reactions are required to provide good wetting of a molten solder, to form metallurgical bond to wettable surfaces, and thereby to yield a decent joint strength. Factors such as intermetallic compound (IMC) formation, IMC spalling, UBM dissolution, interfacial void formation, all affect the integrity and reliability of solder joints. The failure mechanisms identified in thermal fatigue or electromigration stressing of solder joints are often influenced by the interfacial reactions.

When Sn-rich solders are used for Pb-free applications, the interfacial reactions become more aggressive since Sn-rich solders have a larger Sn content and require a higher reflow temperatures than eutectic Sn-Pb solders. To control the aggressive reactions, a reaction barrier layer, such as Ni, electrolytic or electroless, is commonly used, because Ni has a much less solubility than Cu in molten Sn at the corresponding reflow temperature. The solubility of Cu in Sn is approximately seven times larger than Ni at a reflow temperature of 260°C, and is about five times larger at a typical aging temperature of 150°C [10, 47].

Recently, numerous research works have been performed to control various aspects of the interfacial reactions by adding various minor alloying elements to Sn-rich solders, such as Bi, Co, Cu, Fe, Ge, Mn, Ni, Sb, Ti, Zn, rare-earth metals (Ce, La), and others [9, 12, 14, 16-18, 22, 25-26, 29, 34-36, 42-46, 48-54]. In this section, controlling the interfacial reactions in Pb-free solders is briefly discussed in terms of UBM dissolution, IMC formation, void formation and IMC spalling.

4.1. Dissolution of UBM and Surface Finishes

The interfacial reactions between Sn-rich solders (Sn-3.5Ag, Sn-3.8Ag-0.7Cu, Sn-3.5Ag-3.0Bi) and several surface finishes commonly used in printed circuit boards were investigated in terms of their dissolution kinetics and interfacial IMC growth [55]. Table 10 summarizes the dissolution and IMC growth rates at 250°C up to 20 min reflow. The dissolution rates of Ni-based metallization, (Au/Ni(P) or Au/Pd/Ni(P), are much smaller than that of Cu metallization (about one half at 250°C). It is also noted that the dissolution rate of Ni-based metallization is the least in Sn-3.8Ag-0.7Cu among other solders, suggesting the small amount of Cu in SAC to significantly suppress the Ni dissolution. In the same study, as shown in Table 11, the dissolution kinetics of electroplated Ni is shown to be much slower than the electroless Ni (one half to one third).

In an attempt to reduce the Cu dissolution and void formation during thermal aging, several minor alloying elements, such as Co, Fe, Ni/In, and Zn, were added to the standard Sn-3.0Ag-0.5Cu (SAC305), [26]. Low-level Zn additions to SAC305 are found to be most beneficial in reducing Cu pad consumption, Cu_3Sn phase, and interfacial void formation. The increased Cu content in SAC309 (0.9Cu) is also beneficial to reduce Cu consumption [26].

In a study to control the interfacial reactions with various Ni UBMs (electroless, electrolytic, sputtered), a small amount of Ni (0.2 wt %) was added to Sn-rich solders, intending to saturate to the solubility limit in Sn at 260°C [56]. In addition, an over-layer of thin Cu (0.5 or 1.0 μm) was deposited on Ni UBM to investigate the effects of an additional Cu layer on the interfacial reactions. It is found that the consumption of Ni UBM is significantly reduced by the addition of 0.2 wt % Ni to pure Sn and Sn-2Ag solders, but rather increased in Sn-0.7Cu with Ni(P) or sputtered Ni. A metallurgical explanation for this composition dependence is also discussed. The Ni addition is more effective with Ni alloy UBMs (NiSi, NiW, Ni(P) than pure Ni (electrolytic or sputtered). The Cu over-layer is only beneficial in Sn-0.7Cu, but not in pure Sn and Sn-2Ag.

4.2. Cu-Sn Intermetallic Formation

When a Sn-rich solder is melted (or reflowed) on Cu metallization, the first IMC to be formed at the interface is Cu_6Sn_5, and subsequently the second IMC, Cu_3Sn phase is formed in between Cu_6Sn_5 and Cu. Since the Cu_6Sn_5 phase is formed in contact with a molten solder, it has an irregular morphology (round or jagged), reflecting the liquid-solid reaction, while the Cu_3Sn phase has a planar interface with a rather uniform thickness. Since a solid-state diffusion of Cu

and/or Sn through Cu_6Sn_5 is required to form Cu_3Sn, it is usually much thinner than Cu_6Sn_5. Excessive formation of Cu-Sn IMCs is not desirable because of their brittle nature of mechanical properties, especially, when the relative volume of IMCs to a solder joint become significant, such as flip-chip or micro bumps of 3D interconnects.

An extensive literature is available on the formation of Cu-Sn intermetallics in Pb-free solders/joints for their growth kinetics, mechanisms, morphological evolution, compositional analysis, mechanical/electrical/physical properties, and others [19, 25, 43, 48, 49, 57, 58].

The IMC growth kinetics in Sn-3.8Ag-0.7Cu PBGA joints was investigated as a function of reflow cycle and UBM (Cu vs. Ni(P) [59]. The IMC on Cu UBM grew much thicker (9 to 17 μm) than on Ni(P) UBM (4 to 6 μm) after 12 reflows at 260^oC (peak temperature), as summarized in Table 12. When a Cu UBM was coupled with a Ni(P) at an opposite interface, the growth of IMC layers formed on both interfaces were enhanced compared to the case of having the same UBM on both sides. This suggests the UBM on one side strongly influences the IMC growth on the opposite interface in multiple reflows.

Minor addition of Zn to Sn-3.8Ag-0.7Cu was found to be very effective in reducing the IMC growth on Cu pads in multiple reflows, while the effect was not significant for Au/Ni(P) [25]. The Cu-Sn IMC growth during high temperature aging at 150^oC was also reduced in Zn-added SAC, especially for the second Cu_3Sn layer. Retardation of the Cu-Sn IMC layers during reflow and aging was attributed to the accumulation of Zn atoms at the Cu_3Sn and Cu interface [25].

In another study, the influence of low level doping of Co, Cu, Fe, Ni/In and Zn to SAC 305 was investigated with BGA solder joints thermally aged at 150^oC up to 2000 h [26]. Table 13 summarizes the results on IMC thickness and Cu pad consumption for each minor alloying element in comparison with SAC305. The Cu consumption was significantly reduced by the addition of Zn, Cu, or Fe, but rather increased with Co or Ni/In. The Cu_3Sn thickness was significantly reduced by the addition of Zn, Co, Fe, or Ni/In, while it was similar with SAC309. The Zn addition was most effective in reducing the total IMC thickness as well as the Cu_3Sn thickness after 2000h aging at 150^oC among other alloying elements examined.

Minor Ni addition to Sn-3.5Ag was reported to increase the Cu dissolution and to enhance the growth of $(CuNi)_6Sn_5$ during reflow, but to suppress the growth of Cu_3Sn during solid-state aging [60]. The reduced growth of Cu_3Sn was regarded to be beneficial to suppress the Kirkendall voids and thereby to improve the impact strength of the corresponding joint. However, in a search for the 4th element addition to Sn-Ag-Cu solders to improve the high temperature aging resistance, the Ni addition was not favorably recommended, because it could cause a brittle failure or reduction in the impact strength after high temperature aging [61].

The beneficial effects of minor Ti or Mn addition were reported with SAC joints by controlling their microstructure, improving drop impact strength as well as suppressing the interfacial IMC growth [62].

The beneficial effects of minor Zn addition (0.1 to 0.7 wt %) to Sn-Cu and Sn-Ag-Cu solders were systematically investigated with various Cu substrates, such as high-purity Cu, oxygen-free Cu, electroplated Cu and sputtered Cu [63]. Fig. 6 shows typical cross-sectional images of Sn-3.8Ag-0.7Cu, and Sn-3.8Ag-0.7Cu-(0.1, 0.4, 0.7)Zn solders on electroplated Cu after the reflow and aging for 500 h and 1000 h at 150°C. The thickness of Cu-Sn IMC layers was plotted as a function of Zn content in SAC, as shown in Fig. 7. In general, the thickness of each IMC decreases as the Zn content increases. All IMCs of SAC-0.7Zn are much thinner than others, especially for Cu_3Sn. The 0.4 wt % addition was recommended to control the IMC growth as well as the interfacial void formation with electroplated Cu substrates, which were prone to void formation upon high temperate aging at 150°C [63].

The beneficial effects of Zn addition on the interfacial reactions were earlier explained by observing accumulation of Zn atoms at the interface between Cu_3Sn and Cu after multiple reflows, employing the high-resolution TEM/FIB technique combined with EDX [25]. Fig. 8 exhibits a representative image of the interfacial region in a SAC+0.7Zn solder joined to a Cu pad. The ion-beam image clearly shows the well-known double-layer structure of Cu_6Sn_5 and Cu_3Sn formed on top of the Cu pad. The IMC layer attached to Cu, Cu_3Sn is very thin, less than 1 μm thick, even after 10 reflows, while the Cu_6Sn_5 in contact with the solder has progressively grown to a few micron thickness. The EDX analysis was conducted across the IMC interfaces to identify the IMC

layers as well as any segregation of Zn atoms. As shown in Fig. 9, an accumulation of Zn atoms at the interface between Cu and Cu3Sn layer was noted [25].

To further reveal the amount and location of Zn atoms dissolved in the IMC layers, the Zn-accumulated regions in Sn-0.7Cu-0.4Zn joints after aging at 150°C were re-investigated by the high-resolution STEM micro-analysis [43]. Fig. 10 shows a typical example of a high resolution TEM image of the interface between Sn-0.7Cu-0.4Zn and electroplated Cu aged at 150°C for 1000 h. The micro-analysis of EDS results of the regions, (a), (b), (c), (d) and (e) marked in Fig. 10 are also tabulated in Fig. 10. A significant level of Zn accumulation, 1-2 wt %, was detected in the regions of (b), (c) and (d), which correspond to the interface between Cu_3Sn/Cu, the layer of Cu_3Sn, and the Cu_6Sn_5 layer, respectively. In addition, an appreciable amount of Zn atoms, 0.8 wt %, was also detected in the region (a) of the Cu substrate underneath the Cu_3Sn layer. The results strongly support that Zn atoms exist in Cu-Sn IMCs or Cu-Zn solid-solution, not in a form of Cu-Zn IMCs [63]. In addition, a thermodynamic calculation for the driving force to form the Cu_3Sn phase as a function of Zn content at 150°C in the Sn-Cu-Zn system was conducted to explain the reduced growth of Cu_3Sn layer in Zn-added solders [43].

4.3. Interfacial Void Formation

The formation of voids between the interfacial IMCs and Cu substrate has been well recognized as an important reliability issue affecting the integrity of Pb-free solders joints [22-24, 64]. The void formation is possibly caused due to an imbalance in atomic flux across the diffusing interface, that is, Cu atoms diffuse out faster across the Cu-Sn IMC layer(s) toward the solder than Sn atoms diffuse through the IMCs from the Sn-rich solder. This phenomenon is known as the Kirkendall effect, which was originally observed to occur during an interdiffusion experiment between Cu and Cu-Zn alloy, where Zn atoms diffuse faster than Cu atoms across the interface [65].

Upon an extended annealing of SAC joints in contact with Cu, at 150ºC, voids were observed at the interface between Cu and IMCs, and could grow and coalescence into a void layer as the annealing progresses [23]. This void structure would drastically reduce the impact drop strength of Pb-free solder joints [23]. Accordingly, several approaches have been proposed to improve the impact reliability of Sn-rich solder joints. Among these are the placement of a diffusion barrier layer over Cu, such as electroless Ni(P) or electroplated Ni [22], and additions of

minor alloying elements into the SAC alloys to control the IMC growth [18, 22] or to suppress the interfacial void formation [17, 25, 26, 52].

In the efforts to maintain the solder joint shear strength and ductility after an extended high temperature aging, several minor alloying elements, such as Co, Fe, Mn, Ni, Ge, Ti, Si, Cr, and Zn, were added to modify a strong (high Cu content) SAC solder alloy [52, 61]. Of the choices tested, Co, Fe, and Zn substitutions for Cu were found to be attractive in terms of IMC segregation effects, suppression of IMC growth and void formation, and mechanical properties of joints [61], while the Ni addition was not recommended based on the brittle fracture observed in shear test. By using the WDS (wave-length dispersive spectroscopy) technique, it was also demonstrated the interfacial segregation of minor alloying elements of Fe, Co or Zn at the joint interfaces after 1000 h aging at 150C [61], consistent with the similar findings [25, 43].

As discussed earlier, a small addition of Zn to SAC significantly reduced the growth of a Cu_3Sn IMC layer, and thereby the formation of interfacial voids during the solid-state annealing, when in contact with Cu metallization [25, 26, 63]. Fig. 11 displays an example of void formation at the interfacial regions of electroplated Cu substrates reacted with or without Zn additions. Several voids are noted in the Cu_3Sn phase, while no voids were detected in the Zn-added solders [63].

In order to estimate the propensity of void formation, the average distance between voids was measured with SAC solders of several minor alloying elements, such as Co, Cu, Fe, and Zn, aged at 150°C, up to 2000 h, as tabulated in Table 14 [26]. The Zn addition almost completely suppressed the void formation compared to other minor alloying elements after the aging of 2000 h. It is also interesting to note that SAC309 has 50% more voids for 1000 h aging, while the difference became insignificant for the longer aging time of 2000 h.

4.4. Spalling of Ni-Sn Intermetallics

Recently, electroless Ni(P) metallization has received great attention as a reaction barrier layer for Pb-free solder joints, because of its low cost and simple processing steps. However, the interfacial reactions with Ni(P) are more complex than electroplated Ni, owing to the formation of a P-rich layer between the Ni-Sn IMC and Ni(P) during reflow and solid-state annealing [66-69].

Spalling of Ni-Sn IMCs from the interface is commonly observed when the interfacial reactions progress [68-71]. The IMC spalling was found to be strongly influenced by P content, solder volume or deposition method [70]; higher P content and larger solder volume causing more spalling. In addition, a higher tendency of IMC spalling was noted from screen printed solder paste over electrodeposited solder .It was also determined that the solder-deposition method (plating vs. solder paste) was important to the IMC spalling behavior. Upon reflow, solder paste reflowed causes more spalling than electroplated solder under equivalent conditions [68]. The IMC spalling from a Ni(P) layer is also closely related to the crystallization process. A Ni-Sn-P layer forms between Ni_3Sn_4 and crystalline Ni_3P, causing Ni-Sn IMC spalling to occur from the Ni-Sn-P surface [68]. The IMC spalling becomes less severe from a Ni(P) layer when Sn-rich solders contain a small amount of Cu, possibly by altering the structure or composition of Ni-Sn IMCs [55, 57, 69].

To prevent IMC spalling, a thin intermediate layer of Sn or Cu was deposited on top of Ni(P) by electro- or electroless plating. During the reflow reaction of Sn-3.5%Ag solder paste, the intermediate layers effectively suppressed Ni-Sn IMC spalling during the reflow reaction at 250°C, 30 min, while most IMC already spalled off the Ni(P) in a few minutes in the control samples without an intermediate layer [71]. The Sn layer provided protection of the Ni(P) surface and a good wettable surface during reflow. The thin Cu layer changed the chemical structure of the interfacial IMCs in addition to providing a good wettable surface.

5. Modifying the Microstructure of SAC

The microstructure of a solder joint is determined by the complex interplay among several factors such as solder composition, solidification conditions (reflow temperature, dwell time, cooling rate, etc), solder volume, minor alloying elements, UBM, and others. A typical microstructure of a ternary Sn-3.8Ag-0.7Cu alloy in a BGA solder joint is a non-equilibrium one as shown in Fig.1, consisting of Sn dendrite cells surrounded by a network of fine intermetallic particles of Ag_3Sn and Cu_6Sn_5. Occasionally, the large primary Ag_3Sn plates and/or Cu_6Sn_5 rods may be found as noted in Fig. 1. A large amount of undercooling required for Sn solidification promotes growth of the primary phases once nucleated in a undercooled liquid, by prolonging their growth time until the solidification is completed. The large undercooling is also responsible for the large grain structure commonly observed in Sn-rich solder joints [15, 28, 72, 73]. When a solid

phase nucleates in a significantly undercooled liquid Sn, the solidification process occurs in a very short time and its latent heat released becomes large enough to heat up the melt and thereby to make additional nucleation difficult. This situation would lead to form a large grain microstructure of one or a few grains.

The grain structure observed in Sn-Ag-Cu solders is often related with cyclic twinning orientations. Two different cyclic twinning morphologies have been observed [28, 73]; a twining structure of 60° rotations with 3 dominant twin orientations cyclically repeating around the nucleus (known as Kara's beach ball structure), and a highly interpenetrating dendrite structure with no well-defined twin regions [74]. It is also reported that Sn grain size in Sn-Ag-Cu solders significantly increases as Cu content increases from 0 to 1.1%, while the Ag addition to Sn decreases the grain size of Sn-Ag [73].

The microstructure and mechanical properties of binary Sn-Cu and Sn-Ag solders were systematically investigated in terms of their composition and cooling rate [72]. Fig. 12 exhibits the microstructure variations in Sn-Ag solders revealed by cross-polarized light microscopy. The grain size of Sn-xAg (x= 0, 0.5, 1.0, 1.8 wt %) solders generally increases as the cooling rate is reduced from the quenched rate (~$100^oC/s$) to the air cooled (~$10^oC/s$) to the furnace cooled (~$0.02^oC/s$), while the grain size of pure Sn appears to be independent of cooling rate. A small addition of Ag is found to be very effective to reduce Sn grain size, especially in the quenched condition. In the quenched Sn-0.5Ag samples, about 50% of solder balls has the fine grain structure, while the remaining ones have one or a few grains. As the Ag content increases, the ratio of having the fine grains increases. For the quenched Sn-1.8Ag, over 90% have the fine grain structure. The similar fine grain structure was also observed in high Ag or near-ternary eutectic Sn-Ag-Cu solders [73, 74]. For low Ag solders, the microstructure is more sensitive to Ag content than cooling rate [72]. The fine grain structure in the quenched sample of Sn-0.5%Ag was analyzed by EBSD and found a mixture of cyclic twins (with 60° misorientation) and low angle boundaries, not general grain boundaries [72]. The propensity of forming fine cyclic twins in Sn-Ag solders was explained by noting a large supersaturation of Ag atoms in the quenched Sn matrix compared to Sn-Cu solders from the thermodynamic data of their solubility in Sn [72].

To compare the alloying effects of Ag versus Cu in Sn-rich solders, the microstructure of Sn-xCu (x= 0, 0.5, 1.0, 1.5, 2.0 wt %) was investigated in terms of Cu content and cooling, as shown in Fig. 13. In the quenched condition, contrary to Ag, the Cu addition did not produce any fine grain microstructure at all, while the grain size generally decreases as Cu content increases for

the air cooled and the furnace cooled case. The microstructure of low Cu solders (0.5 and 1.0 wt %) is pretty similar to pure Sn of large grains, not sensitive to its cooling rate. Another interesting feature was reported on the Sn grain orientations of the fine grain structure observed such as in Sn-2.0Cu by the EBSD analysis [72]. The misorientation between neighboring grains was distributed over a wide range of 0 to 95 deg, indicating the fine grain structure being general grain boundaries, not related to the twinning structure as observed in Sn-Ag solders. The microstructure (or Sn grain size) in Sn-Cu solders was found to be closely related to the distribution of Cu_6Sn_5 particles, which are strongly influenced by both Cu content and cooling rate.

Another important effect of Cu content reported is on the pasty range of SAC solder joints [35]. The pasty range is defined as the difference between the liquidus and solidus temperature of a given alloy composition. It is desirable to have a smallest pasty range possible to reduce the defect rate in solder joints. The pasty range of SAC solder joints is quite sensitive to Cu content, above the eutectic composition, but not to Ag content. For Ag contents ranging from 2.1 to 2.7%, the pasty range is estimated to be 2 to 4°C for 0.7%Cu and 15 to 17°C for 0.9%Cu. Comparing the microstructure of Sn-3.5%Ag [76] with the near-eutectic ternary SAC alloys [75], it is noted that the presence of Cu in SAC alloys promotes more dendrite growth of β-tin.

The effect of Zn addition to SAC was investigated to control the formation of large Ag_3Sn plates [14, 77]. It was also reported that Zn additions modified the microstructure of the β-tin dendrite, as well as the ternary eutectic microstructure. For Zn-added solders, Sn dendrites become coarser and the volume fraction of the eutectic phase increases at an equivalent cooling rate. Considering Zn atoms preferentially react with Cu atoms, the role of Zn is regarded to influence the nucleation of the eutectic microstructure and thereby to promote the formation of the eutectic microstructure. Since Zn can be easily oxidized in a molten solder and can hence degrade solder wettability, the amount of Zn addition should be limited to a minimum and the reflow process is required to be performed in an inert atmosphere, such as nitrogen.

A minute amount of Ni and Ge additions to Sn-0.7Cu solders has been practiced to improve soldering characteristics, fluidity, to reduce shrinkage defects, to reduce the volume fraction of Sn dendrite and to promote a more-eutectic microstructure, [78-80].

The additions of rare earth metals, such as Ce, La, or Y, have been reported to improve wettability, creep strength and tensile strength, and to refine the microstructure of Pb-free solder joints [81-85]. The addition of a small amount of La (up to 0.5 wt %) to SAC refined the microstructure by decreasing the length and spacing of Sn dendrites and decreased the interfacial Cu-Sn IMC thickness [82], which significantly enhanced its elongation with a small decrease in shear strength. In addition, some refinement of Sn grain size and IMC particles was also reported [83, 84]. However, in case of Ce-added SAC, abnormal Sn whisker growth was reported even after 1 day at an extremely high growth rate (~8.6A/sec) [85]. The high growth rate was owing to Sn whisker formation from the oxidizing $CeSn_3$ phase.

The influence of the interfacial reactions on the microstructure of solder joints was reported [86]. When Sn-Ag and Sn-Cu solders are reacted with Cu or Ni(P) UBM, Cu and Ni atoms dissolve quickly to saturate to their solubility limits in molten solders, causing the changes in composition and microstructure. A few large grains in pure Sn and Sn-0.5Cu solders change to many columnar grains after reacted on a Cu UBM, influenced by the large increase in Cu content(~1.3 wt %). In contrast, when reacted on Ni(P), a few large grains are maintained, probably due to the small increase in Ni content (~0.07 wt %). The fine twins in Sn-Ag solders also changed to a few large grains after reacted with Cu or Ni(P) UBM. This microstructure change is attributed to the compositional changes during reflow and the accompanied precipitation of IMC particles in solder joints [86].

6. Improving Mechanical Properties

6.1. Strength and Hardness

The mechanical properties of Pb-free solders and joints have been extensively investigated in terms of alloying elements, solidification conditions or other processing parameters [4, 8, 12, 15-17, 59, 72, 75, 76, 87]. Several Pb-free solders were evaluated as a function of alloying composition, plastic deformation and annealing condition [87]. The strain hardening behavior of Sn-rich solders is significantly affected by the amount of alloying elements and plastic deformation. More plastic deformation and more alloying elements yield larger strain hardening, confirmed by their microhardness measurement. However, pure Sn does not exhibit substantial strain hardening, due to the recrystallization and grain growth occurring at room temperature. For high solute solders, such as Sn-3.5Ag and Sn-3.5Ag-0.7Cu, recrystallization requires both a considerable amount of plastic deformation, such as 30% or higher, and an annealing condition, such as 150°C for 48 h. This confirms that high-solute solders of SAC have a better microstructure stability than low-solute solders, such as Sn-0.7Cu or pure Sn [87].

High-solute solders or near-ternary eutectic Sn-Ag-Cu solders are usually not chosen for flip-chip applications, because they have high modulus and high tensile strength. Recently, low-Ag solders become popular for the solder interconnects required for low strength and high ductility. Fig.14 exhibits the microhardness data of low solute solders, Sn-Ag and Sn-Cu, measured in terms of alloy composition and cooling rate [72]. Sn-Cu solders follow a general structure-property relationship, that is, a higher hardness for more alloy additions and faster cooling. However, Sn-Ag solders do not follow this relation in regard with cooling rate; the air-cooled solders exhibit a higher hardness than the rapidly quenched, as shown in Fig. 14 (a). Sn-Ag quenched solders have a fine twin structure, while Sn-Ag air-cooled have a relatively coarse microstructure revealed by the cross-polarized images in Fig. 12. Generally, for metals and alloys a finer grain structure is responsible for a higher yield strength (or higher hardness) due to the grain boundary strengthening mechanism (known as Hall-Petch relationship). But the fine twin structure observed in Sn-Ag solders seems to not contribute for the hardening of Sn-rich solders. Further, it is reported that the microhardness data of Sn-Ag and Sn-Cu are better correlated with the characteristics of IMC particles (quantity, size, distribution) rather than Sn grain or twin size revealed in cross-polarizing images [72].

Comparing the hardness data of Sn-Ag and Sn-Cu solders, it is evident that the addition of Cu solute atoms to Sn matrix is much more effective than Ag to Sn at the same cooling rate as shown in Fig. 14. This is explained by two reasons. First, the volume fraction of Cu_6Sn_5, formed at 220°C, just below the eutectic temperature, is estimated to be always larger than Ag_3Sn for the same wt % of Cu or Ag [72]. The second reason is such that the bulk hardness of Cu_6Sn_5 (~4.5GPa) is much higher than Ag_3Sn (~1.5GPa) [88]. Hence, for the same amount of Ag or Cu, Sn-Cu solders are expected to be harder than Sn-Ag, assuming each IMC system has a similar size and distribution characteristics.

6.2. Drop Impact Resistance

Drop impact resistance is an important reliability issue for Pb-free solders joints, especially for mobile electronics. The brittle fracture of solder joints during drop impact test is often caused by the weak interface owing to the formation of voids along IMC layers [23]. To improve the drop impact resistance of Pb-free solder joints, two approaches have been taken; reducing Ag or Cu content in SAC solder to increase the ductility of the solder matrix [89-91], and/or adding minor alloying elements to suppress the interfacial void formation and IMC growth [52, 58, 62, 78, 89, 90].

A small addition of Ti, Mn, Ni, or In is also reported to improve the impact resistance of Sn-Ag-Cu joints [62, 90], while Ni and Ge are added to Sn-Cu [78], or Zn added to Sn-Ag-Cu or Sn-Cu for the same purpose [25, 43]. Examples of void suppression by Zn addition to Sn-Cu or Sn-Ag-Cu are already shown in Fig. 11 [63]. However, when an excessive amount of Zn is added to Sn-rich solders, the drop impact resistance would rather degrade [54].

6.3. Thermal Fatigue Resistance

In the early Pb-free, flip-chip development, thermal fatigue performance of Pb-free solders was compared with Pb-containing solder joints [21, 92-94]. Three Pb-free solders, Sn-0.7Cu, Sn-3.8Ag-0.7Cu and Sn-3.5Ag, formulated as solder paste, were evaluated for flip chip applications [94]. Among the solders and UBM evaluated, Sn-0.7Cu bump on both Ni(P) and TiW/Cu had the longest fatigue life, while Sn-3.5Ag on Ni(P) the shortest life [94]. The Sn-3.8Ag-0.7Cu on TiW/Cu had a better fatigue life than Sn-3.5Ag, worse than Sn-0.7Cu, and a similar life to Sn-37Pb on Ni(P). The better fatigue performance of Sn-0.7Cu joints were explained by the fatigue

crack initiation/propagation mechanism through the grain boundaries. For Sn-0.7Cu joints, the cracks were observed to propagate at the grain boundaries, significantly removed from the UBM/bump interface near the center of the joint. This solder was claimed to be most compliant in thermal fatigue and to undergo massive deformation before failing by crack propagation [93].

The effect of silver content on thermal fatigue life of flip chip interconnects was systematically investigated for the packages assembled to FR-4 substrate with Sn-Ag-Cu solder balls [95]. From the thermal cycling test (between -45 and 125^oC), solder joints with a high Ag content, 3 and 4 wt %, were found to have a longer fatigue life compared to solder joints with a lower Ag content, 1 and 2 wt %. The better fatigue performance of high-Ag solders was attributed to their stable microstructure owing to a uniform dispersion of fine Ag_3Sn particles. In low-Ag joints, significant coarsening of the microstructure was observed during the thermal cycling test [95].

In another study, the effect of Ag content on thermal fatigue life of ceramic BGA modules assembled on an organic substrate was evaluated in terms of Ag content, cooling rate and thermal cycling condition [16, 96]. The fatigue life was influenced by Ag content as well as thermal cycling test condition. The low-Ag joints (2.1%) had the best thermal fatigue life for the thermal cycling test between 0 and 100^oC with a long cycle time of 120 min, while the high-Ag joints (3.8%) had the best life for the short cycle time of 30 min. The slow cooling rate (0.5^oC/s) used during assembly was beneficial to the thermal fatigue life regardless of Ag content or thermal cycling conditions compared to the fast cooling rate (1.7^oC/s).

Since the microstructure of Pb-free BGA or flip chip joints are known to be either a single crystal or composed of a few grains [28, 97], the fatigue performance of Pb-free solder joints would be strongly affected by the crystal orientation of Sn matrix. In the conventional thermal cycling test, solder bumps at the corner of a Si chip or module with the largest DNP would expect to fail first, but this situation would not be warranted when the crystal orientation of Sn matrix plays into the failure process. An example was discussed with Pb-free BGA solder joints, where the c-axis of Sn-crystal was oriented parallel to the substrate direction, premature fails were observed regardless of the position of solder joints [28, 97].

7. Enhancing Electromigration Resistance

Recently, the electromigration (EM) in Pb-free solder joints for flip-chip applications has become a critical reliability challenge, largely because of lower melting temperatures of Sn-rich solders in comparison to high-Pb solders as well as the remarkable anisotropy in diffusion rates of common solute atoms such as Cu, Ni, or Ag in Sn matrix as discussed earlier.

Early EM test results obtained from actual flip-chip solder joints are often complicated to compare each other because their solder temperature and current density significantly vary among samples due to current crowding and local joule heating. In order to avoid these complications, a model wire test structure, providing uniform current density and minimal gradients, was adopted to compare pure electromigration effects of solder composition, UBM, and surface finish [34, 98, 99]. From this study, it was found that Sn-Ag joints have a superior EM performance over Sn-Cu under the same conditions of other variables, as shwon in Fig. 15 [34, 99]. In addition, two failure mechanisms are identified [98]; Mode-I, probably dominated by Sn self-diffusion resulting in separation between IMC and solder. Mode-II is responsible for premature fails in EM tests, which is dominated by a fast diffusion process of Ni and/or Cu in Sn, when the c-axis of Sn grain orientation is parallel to the direction of electron flow. EM failure mechanism in Sn-Ag joints with higher Ag content is dominated by Mode-I fail, while more Mode-II was observed in Sn-Cu joints. In the subsequent study, the alloying effects of Ag, Cu and Zn on the EM performance of Sn-rich solders have been systematically investigated using the Cu wire structure [34, 100]. For Sn-Ag joints, the frequency of early EM fails (associated with Mode-II) significantly decreases as Ag content increases, while Mode-II fails are more commonly observed in Sn-Cu joints for all Cu concentrations tested. The EM lifetime of Sn-Cu joints is generally shorter than Sn-Ag or Sn-Ag-Cu joints. The better EM performance of Sn-Ag over Sn-Cu is explained by the stable network of Ag_3Sn particles during EM or high temperature aging experiment [101].

The beneficial effect of Zn doping on EM performance is also reported for Sn-Ag joints [34, 100]. It is observed that Zn combines closely with Cu and Ag that stabilizes the IMC network and effectively slows down Cu diffusion. Hence, EM reliability is significantly improved in Zn-doped Sn-Ag joints. The effects of other alloying elements such as Ni, Sb or Bi were also investigated, but finding no appreciable improvement on EM performance.

In a recent study, the EM performance of Pb-free solder joints is investigated in terms of solder composition (Sn-0.5Cu vs Sn-1.8Ag) and joining path to Cu or Ni(P) UBM [102]. It is

again confirmed that Sn-Ag joints are superior to Sn-Cu regardless of the choice of UBM and its joining path. For Sn-1.8Ag joined first to Cu UBM, Cu atoms migrate fast through 60o twin boundary under current stressing. However, since Ag atoms hardly migrate to the anode side under current stressing, Sn-1.8Ag joints have a longer EM lifetime than Sn-0.5Cu joints. When Sn-1.8Ag joined first to Ni(P), because of their stable microstructure and initially thicker IMC layers, Cu migration through low-angle boundraies and Sn lattice is much slow and its EM lifetime is enhanced accordingly [102].

8. Summary

Near-ternary eutectic SAC solders are widely used in Pb-free microelectronic applications, such as surface mount or plated-through-hole joints in printed circuit boards, BGA (ball grid array) or CSP (chip scale package), and others. Many variations of near-ternary SAC compositions are available depending on their applications as listed in Table 1.

However, near-ternary SAC compositions are not well implemented for Pb-free solder joints requiring a high ductility, low modulus, or enhanced impact resistance. The applications for mobile electronics and flip-chip interconnect of high performance systems are the few examples of this kind. Here, low-Ag or low-solute SAC solders have been recommended at an expense of stable microstructure and other physical/mechanical properties.

Recently, the anisotropic properties of Sn grain orientations are found to critically affect key reliability performance of Pb-free solder joints, such as electromigration, thermal fatigue, or chip-to-package interaction (CPI). Since the microstructure of small solder joints such as flip chip or BGA consists of a few grains or even a single crystal, the orientation of Sn crystal(s) is crucial in determining the integrity or reliability of solder joints. The fast diffusion of common solute atoms (such as Ag, Cu, Ni) along the c-axis of Sn crystal often causes premature fails of Pb-free flip-chip joints during their electromigration stressing. Moreover, since the elastic constant and CTE (coefficient of thermal expansion) are a few time larger along the c-axis of Sn crystal than the a- or b-axis, this situation provides more challenging technical issues to compromise several important reliability risk factors of Pb-free solder joints.

The addition of minor alloying elements (such as Zn, Co, Fe, Mn, Al, Ti, Ni, and others) to Sn-rich solders is actively being investigated to improve the integrity or reliability of Pb-free solders joints. Among them, Zn addition is most promising and extensively investigated. Some beneficial effects of Zn addition to Sn-rich solders include

1) Suppress large Ag_3Sn plate growth
2) Reduce the undercooling during Sn solidification
3) Suppress IMC growth, especially Cu_3Sn at the Cu/solder interface
4) Reduce void formation at the Cu/Sn IMC interface
5) Reduce Cu consumption during reflow and aging
6) Promote uniform Sn dendrite microstructure
7) Improve drop impact resistance
8) Enhance electromigration resistance

Further research and development activities are needed to fully understand the beneficial effects of minor alloying elements on other important technical issues such as Sn whisker formation, Sn pest transformation, and others.

References

1. B. R. Allenby, et. al., "An Assessment of the Use of Lead in Electronic Assembly," *Proc. Surface Mount Int*., (San Jose, CA), 1, pp.1-28, Aug. (1992).

2. P. Vianco and D. Frear; "Issues in the Replacement of Pb-Bearing Solders," *J. of Metals,* p.14, July, (1993).

3. S. K. Kang and A. Sarkhel, "Lead (Pb)-free Solders for Electronic Packaging," *J. Elec. Materials*, 23(8): p.701, Aug. (1994).

4. J. Glazer, "Microstructure and Mechanical Properties of Pb-Free Solder Alloys for Low-Cost Electronic Assembly: A Review *J. Elec. Mat's*, 23(8), p.693, (1994).

5. I.E. Anderson, "Tin Silver Copper: a lead free solder for broad applications," *Proc. NEPCON West'96 Conf,* Vol. 2, p.882, (1996).

6. S. K. Kang, R.S. Rai, and S. Purushothaman, "Interfacial Reactions During Soldering with Lead-Tin Eutectic and Lead (Pb)-Free, Tin-Rich Solders," *J. Elec. Mater.*, 25(7), p.1113,, (1996).

7. NCMS, "Lead-Free Solder Project Final Report," National Center for Manufacturing Sciences, Report 0401RE96, Ann Arbor, MI, Aug. (1997).

8. R. Ninomiya, K. Miyake, J. Matsunaga, "Microstructure and Mechanical Properties of New Lead Free Solder," *Proc. InterPACK'97*, (Kohala Coast, HI), p.1329, (1997).

9. S. K. Kang, J.Horkans, P.Andricacos, R.Crruthers, J.Cotte, M.Datta, P.Gruber, J.Harper, K.Kwietniak, C.Sambucetti, L.Shi, G.Brouillette and D.Danovitch, "Pb-Free Solder Alloys for

10. K. W. Moon, W. J. Boettinger, U. R. Kitten, F. S. Biancaniello and C. A. Handwerker, "Experimental and thermodynamic assessment of Sn-Ag-Cu solder alloys," J. of Electronic Materials, vol. 29, p.1122, (2000).

11. S. K. Kang, "Recent Progress in Pb-free Solders and Soldering Technologies," J. of the Minerals, Metals and Materials (JOM), p.16, June, (2001).

12. I.E. Anderson, J. C. Foley, B. A. Cook, J. Harringa, R. K. Terpstra, and O. Unal, "Alloying effects in near-eutectic Sn-Ag-Cu solder alloys for improved microstructural stability," J. Elec. Materials, vol.30, pp.1050, (2001)

13, D.W. Henderson, T. Gosselin, A. Sarkhel, S. K. Kang, W.K. Choi, D.Y. Shih, C. Goldsmith, and K. Puttlitz, "Ag3Sn Plate Formation in the Solidification of Near Ternary Eutectic Sn-Ag-Cu Alloys," J. of Materials Research, 17(11), p.2775, (2002).

14. S.K. Kang, D.Y. Shih, D. Leonard, D.W. Henderson, T. Gosselin, S.I. Cho, J. Yu, and W.K. Choi, "Controlling Ag3Sn Plate Formation in Near-Ternary-Eutectic Sn-Ag-Cu Solder by Minor Zn Alloying," *J. The Minerals, Metals and Materials (JOM),* p.34, June, (2004).

15. D. Henderson, J. Woods, T. Gosselin, J. Bartelo, D. King, T. Korhonen, M. Korhonen, L. Lehman, E. Cotts, S.K. Kang, P. Lauro, D.Y. Shih, C. Goldsmith, and K. Puttlitz, "The Microstructure of Sn in Near Eutectic Sn-Ag-Cu Alloy Solder Joints and its Role in Thermomechanical Fatigue," J. Mater. Res.,Vol.19, p.1608, June, (2004).

16. S.K. Kang, P. Lauro, D.Y. Shih, D.. Henderson, J. Bartelo, T. Gosselin, S. Cain, C. Goldsmith, K. Puttlitz, T. Hwang, and W. Choi, "The Microstructure, Thermal Fatigue, and Failure Analysis of Near-Ternary Eutectic Sn-Ag-Cu Solder Joints," Materials Transactions (The Japan Inst of Metals), Vol.45, No.3 p.695, (2004).

17. S.K. Kang, P. Lauro, D.Y. Shih, D.W. Henderson, K.J. Puttlitz, "The Microstructure, Solidification, Mechanical Properties, and Thermal Fatigue Behavior of Lead(Pb)-free Solders and Solder Joints Used in Microelectronic Applications," IBM Journal of Res & Dev, Vol. 49, No. 4/5, p.606, July/Sept, (2005).

18. I.E. Anderson, "Development of Sn–Ag–Cu and Sn–Ag–Cu–X alloys for Pb-free electronic solder applications," J. Elec. Materials, vol.34, p.55, March, (2007).

19. K. Zeng, K.N. Tu," Six cases of reliability study of Pb-free solder joints in electronic packaging technology," Mat's Sci. & Eng, R, v.38, pp.55-105, (2002).

20. J.K. Lin, J.W. Jang, J. White, "Characterization of Solder Joint Electromigration for Flip Chip Technology," Proc. 53rd ECTC, p.816, (2003).

21. J.K. Lin, J.W. Jang, D. Frear, "Lead-Free Flip Chip Interconnect Reliability for DCA and FC-PBGA Packages," Proc. 54th ECTC, p.642, (2004).

22. M. Date, T. Shoji, M. Fujiyoshi, K. Sato, K.N. Tu, "Impact Reliability of Solder Joints" Proc. 2004 ECTC, p.668, (2004).

23. T.C. Chiu, K. Zeng, R. Stierman, D. Edwards, K. Ano, "Effect of Thermal Aging on Board Level Drop Reliability for Pb-free BGA Packages," Proc. 54th ECTC, p.1256, (2004).

24. Z. Mei, M. Ahmad, M. Hu, and G. Ramakrishna, "Kirkendall Voids at Cu/Solder Interface and Their Effects on Solder Joint Reliability," Proc. 55th ECTC, p.415, (2005).

25. S.K. Kang, D. Leonard, D. Y. Shih, L. Gignac, D.W. Henderson, S. Cho, J. Yu, "Interfacial Reactions of Sn-Ag-Cu Solders Modified by Minor Zn Alloying Addition," J. Electron. Mater., vol.35 (3), p.479, (2006).

26. I. de Sousa, D.W. Henderson, L. Patry, S.K. Kang, D.Y. Shih, "The Influence of Low Level Doping on the Thermal Evolution of SAC Alloy Solder Joints with Cu Pad Structures" Proc. 56th ECTC, p.1454, (2006).

27. K.L. Lin, S.M. Kuo, "The Electromigration and Thermomigration Behaviors of Pb-free Flip Chip Sn-3Ag-0.5Cu Solder Bumps," Proc. 56th ECTC, p.667, (2006).

28. T.R. Bieler, H. Jiang, L.P. Lehman, T. Kirkpatrick, E.J. Cotts, "Influence of Sn Grain Size and Orientation on the Thermomechanical Response and Reliability of Pb-free Solder Joints," 46th ECTC Proc., p.1462, (2006)].

29. S.K. Kang, M.G. Cho, P. Lauro, D-Y Shih, "Critical Factors Affecting the Undercooling of Pb-free, Flip-chip Solder Bumps and In-situ Observation of Solidification Process," Proc. 2007 ECTC, pp.1597-1603, Reno, NV, May (2007)

30. B.F. Dyson, T.R. Anthony, and D. Turnbull, *J. Appl. Phys.* 37, 3408 (1967).

31. D.C. Yeh and H.B. Huntington, *Phy. Rev. Lett.* 53(15), 1469 (1984).

32. F.H. Huang and H.B. Huntington, *Phys. Rev. B* 9(4), 1479 (1974).

33. P. Gruber et al., "Low Cost Wafer Bumping", *IBM J. Res. & Dev.* Vol. 49 No. 4/5, p.621, (2005)

34. M. Lu, P. Lauro, D-Y Shih, S.K. Kang, S.H. Chae, S.K. Seo, "The Effects of Cu, Ag Compositions And Zn Doping on the Electromigration Performance of Pb-Free Solders," Proc. 59th ECTC, p.922 (2009).

35. S.K. Kang, W.K. Choi, D.Y. Shih, D.W. Henderson, T. Gosselin, A. Sarkhel, C. Goldsmith, K.J. Puttlitz, "Formation of Ag3Sn Plates in Sn-Ag-Cu Alloys and Optimization of their Alloy Composition," *Proc. 53rd ECTC,* p.64, (2003).

36. S.K. Kang, W.K. Choi, D.Y. Shih, D.W. Henderson, T. Gosselin, A. Sarkhel, C. Goldsmith, K.J. Puttlitz, "Ag3Sn Plate Formation in the Solidification of Near Ternary Eutectic Sn-Ag-Cu Alloys," J. The Minerals, Metals and Materials (JOM), Vol.55, p.61, June, (2003).

37. D. Mis, "Unitives' Plated Pb-free Solder Solution," presented at *Symposium on Peaks in Pacakaging*, October, (2003).

38. R. Kinyanjui, L.P. Lehman, L. Zavalij, and E. Cotts, "Effect of sample size on the solidification of temperature and microstructure of SnAgCu near eutectic alloys", J. Mater. Res., Vol.20, No. 11, Nov.2006, pp.2914-2918.

39. S. K. Kang, Peter Gruber and Da-Yuan Shih, "An Overview of Pb-free, Flip-Chip Wafer Bumping Technologies," JOM, 2008, June, p.66, (2008).

40. S. K. Kang, M.G. Cho, P. Lauro, D-Y Shih, "Study of the Undercooling of Pb-free, Flip-chip Solder Bumps and In-situ Observation of Solidification Process", J. Mater. Res., Vol.22, No.3, p.557, Mar. (2007).

41. M.G. Cho, S.K. Kang, and H.M. Lee, "Undercooling and Microhardness of Pb-free Solders on Various UBMs," J. Materials Research, Vol.23, No.4, p.1147, (2008).

42. M.G. Cho, S.K. Kang, S.K. Seo, D.Y. Shih, and H.M. Lee, "Effects of Under Bump Metallization and Nickel Alloying Element on the Undercooling Behavior of Sn-Based, Pb-free Solders," J.Mater. Res., Vol.24, No.2, p.534, Feb. (2009).

43. M. G. Cho, "Effects of Zn Addition on Undercooling of Pb-free Solder Alloys and Their Interfacial Reactions with Cu and Ni-P UBMs," Ph.D. Thesis, Dept. of Mat's Sci. & Eng., KAIST, Daejeon, Korea, Nov.20, (2008).

44. I.E. Anderson, J.W. Walleser, J.L. Harringa, F. Laabs, A. Kracher, "Nucleation Control and Thermal Aging Resistance of Near-Eutectic Sn-Ag-Cu-X Solder Joints by Alloy Design," J. Elec. Mat's, vol.38 (12), p.2770-2779, (2009).

45. G.G. Hougham, K.K. Srivastava, S.K. Kang, D-Y Shih, B.R. Sundlof, S.J. Chey, D.W. Henderson, D.R. Di Milla, R.P. Ferlita, R.A. Carruthers, "Method and Process for Reducing Undercooling in a Lead-free Tin-rich Solder Alloy," US Pat.#7,703,661B2, issued Apr.27, (2010).

46. M.G. Cho, H.Y. Kim, S.K. Seo, H.M. Lee, "Enhancement of Heterogeneous Nucleation of b-Sn Phases in Sn-rich Solders by Adding Minor Alloying Elements with Hexagonal Closed Packed Structures," Appl. Phys. Lett, vol.95, 021905, (2009).

47. G. Ghosh, "Thermodynamic Modeling of the Nickel-Lead-Tin System," Metall. Mater. Trans. A, 30A, pp. 1481-1494, (1999).

48. J.Y. Tsai, C.R. Kao, "The Effect of Ni on the Interfacial Reaction between Sn-Ag Solder and Cu Metallization," Proc 4th International Symposium on Electronic Materials and Packaging, Kaohsiung, Taiwan, Dec. p. 271, (2002).

49. W.K. Choi, J.H. Kim, S.W. Jeong, H.M. Lee, "Interfacial Microstructure and Joint Strength of Sn-3.5Ag-X (X=Cu, In, Ni) Solder Joint," J. Mater. Res., Vol. 17, No. 1, p.43, (2002).

50. D.Q. Yu, J. Zhao, L. Wang, "Improvement on the Microstructure Stability, Mechanical and Wetting Properties of Sn-Ag-Cu Lead-free Solder with the Addition of Rare Earth Elements," J. Alloys and Comp., Vol. 376, No. 1/2, p.170, (2004).

51. K.S. Kim, S.H. Huh, K. Suganuma, "Effects of Fourth Alloying Additive on Microstructure and Tensile Properties of Sn-Ag-Cu and Joints with Cu," Microelectron. Reliab., Vol. 43 p.259, (2003).

52. I.E. Anderson, J.L. Harringa, "Suppression of Void Coalescence in Thermal Aging of Tin-Silver-Copper-X Solder Joints," J. Electron. Mater., Vol. 35, No. 1, p.94, (2006).

53. M.J. Rizvi, Y.C. Chan, C. Bailey, H. Lu, M.N. Islam, "Effects of Adding 1 wt% Bi into the Sn-2.8Ag-0.5Cu Solder Alloy on the Intermetallic Formation with Cu Substrate during

Soldering and Isothermal Aging," J. Alloys and Comp., Vol. 407, No. 1/2, p.208, (2006).

54. Y.K. Jee, J. Yu, Y.H. Ko, "Effects of Zn Addition on the Drop Reliability of Sn-3.5Ag-xZn/Ni(P) Solder Joints," J. Mater. Res., Vol. 22, No. 10, p.276, (2007).

55. S.K.Kang, D.Y.Shih, K.Fogel, P.Lauro, M.J.Yim, G.Advocate, M.Griffin, C.Goldsmith, D.W.Henderson, T.Gosselin, D.King, J.Konrad, A.Sarkhel, K.J.Puttlitz, "Interfacial Reaction Studies on Lead (Pb)-Free Solder Alloys", IEEE Trans. Elec. Pack. Manuf., Vol.25, No.3, p.155, July, (2002).

56. S K. Kang, M.G. Cho, D-Y Shih, S.K. Seo, H.M. Lee, "Controlling the Interfacial Reactions in Pb-free Interconnections by Adding Minor Alloying Elements to Sn-rich Solders," Proc. 58th ECTC, Orlando, FL, p.478, (2008).

57. W.K. Choi, S.K. Kang, Y.C. Sohn, D.Y. Shih, "Study of IMC Morphologies and Phase Characteristics Affected by the Reactions of Ni and Cu Metallurgies with Pb-Free Solder Joints," Proc. 53rd Elec. Comp. & Tech Conf, New Orleans, LA, CA, p.1190, (2003).

58. W.T. Chen, C.E. Ho, C.R. Kao, "Effects of Cu Concentration on the Interfacial Reactions between Ni and Sn-Cu Solders," J. Mater. Res, Vol.17, No.2, p.263, (2002).

59. S.K. Kang, W.K. Choi, D.Y. Shih, P. Lauro, D.W. Henderson, T. Gosselin, D.N. Leonard, "Interfacial Reactions, Microstructure and Mechanical Properties of Pb-Free Solder Joints in PBGA Laminates," Proc 52nd Elec. Comp. & Tech Conf, San Diego, CA, p. 147, (2002).

60. C.E. Ho, S.C. Yang, C.R. Kao, "Interfacial Reaction Issues for Lead-free Electronic Solders," J. Materials Science, p.155, (20007).

61. I. E. Anderson, "Development of Sn-Ag-Cu and Sn-Ag-Cu-X Alloys for Pb-free Electronic Solder Applications," J. Mater. Sci.; Mater Electron, Vol.18, pp.55-76, (2007).

62. W. Liu, P. Bachorik, N.C. Lee, "The Superior Drop Test Performance of SAC-Ti Solders and its Mechanism," Proc. 58th ECTC, p.452, (2008).

63. M.G. Cho, S.K. Kang, D.-Y. Shih, H.M. Lee, "Effects of Minor Addition of Zn on Interfacial Reactions of Sn-Ag-Cu and Sn-Cu Solders with Various Cu Substrates during Thermal Aging," J. Electron. Mater., Vol. 36, No. 11, p.1501, (2007).

64. P.Borgesen, L. Yin, R. Kondos, D.W. Henderson, G. Servis, J. Therriault, J. Wang, K. Srihari, "Sporadic Degradation in Board Level Drop Reliability – Those Aren't All Kirkendall Voids!", Proc. 2007 ECTC, p.136, (2007).

65. E. Kirkendall, L. Thomassen, and C. Upthegrove, "Rates of Diffusion of Copper and Zinc in Alpha Brass," Trans. AIME, 133, pp. 186-203, (1939).

66. K.N. Tu, A.M. Gusak, M. Li, "Physics and Materials Challenges for Lead-free Solders," J. Appl. Phys, Vol.93, No.3, p.1335, (2003).

67. Y. C. Sohn, Jin Yu, S. K. Kang, W. K. Choi, D. Y. Shih, "Study of the Reaction Mechanism Between Electroless Ni-P and Sn and its Effect on the Crystallization of Ni-P," J. Mat's Res, Vol.18, No.1, p.4, (2003).

68. Y. C. Sohn, J. Yu, S.K. Kang, D.Y. Shih, T.Y. Lee, "Study of Spalling Behavior of Intermetallic Compounds During the Reaction Between Electroless Ni(P) Metallization and Lead-free Solders," Proc. 54th Elec Comp & Tech Conf, Las Vegas, NV, p. 75, (2004).

69. W. Paik, Y.D. Jeon, M.G. Cho, "Interfacial Reactions and Bump Reliability of Various Pb-Free Solder Bumps on Electroless Ni-P UBMs," Proc. 54th ECTC, p.675, (2004).

70. Y.C. Sohn, Jin Yu, S.K. Kang, D.Y. Shih, and T.Y. Lee, "Spalling of Intermetallic Compounds During the Reaction between Lead-free Solders and Electroless Ni-P Metallization," J. Materials Research, Vol.19, No.8, p.2428, (2004).

71. Y.C. Sohn, J. Yu, S.K. Kang, D.Y. Shih, T.Y. Lee, "Effect of Intermetallics Spalling on the Mechanical Behavior of Electroless Ni(P)/Pb-free Solder Interconnection," Proc. 55th ECTC, p.83, (2005).

72. S.K.Seo, S.K. Kang, D-Y Shih, H.M. Lee, "An Investigation of Microstructure and Microhardness of Sn-Cu and Sn-Ag Solders as a Function of Alloy Composition and Cooling Rate," J. Electronic Materials, Vol.38, No.2, pp.257-265, (2009).

73. L.P. Lehman, S.N. Athavale, T.Z. Fullem, A.C. Giamis, R.K. Kinyanjui, M. Lowenstein, K. Mather, R. Patel, D. Rae, J. Wang, Y. Xing, L. Zavalij, P. Borgesen and E. J. Cotts, "Growth of Sn and Intermetallic Compounds in Sn-Ag-Cu Soler", J. Elec. Mat's, Vol.33(12), p.1429, (2004).

74. A.U. Telang, T.R. Bieler, J.P. Lucas, K. N. Subramanian, L. P. Lehman, Y. Xing, E. J. Cotts, "Grain-boundary character and grain growth in bulk tin and bulk lead-free solder alloys", J. Elec. Mat's, Vol.33(12), p.1412, (2004).

75. P.T. Vianco, J.A. Rejent, J.J. Matin : "The compression stress-strain behavior of Sn-Ag-Cu solder," JOM, 55(6), June, 2003, pp.50-55.

76. F. Ochoa, J.J. Williams, N. Chawla, "The effects of cooling rate on microstructure and mechanical behavior of Sn-3.5Ag solder," JOM, 55(6), June, 2003, pp.56-60.

77. K. L. Buckmaster, J.J. Dziedzic, M.A. Masters, B.D. Poquette, G.W. Tormoen, D. Swenson, D.W. Henderson, T. Gosselin, S.K. Kang, D.Y. Shih, K.J. Puttlitz: presented at the TMS 2003 Fall Meeting, Chicago, Nov. 2003.

78. T. Sawamura, H. Komiya, t. Inazawa, F. Nakagawa, "Pb-free Soldering Alloy", US Patent No.6,692,691 B2, Feb. 17, (2004).

79. N. Nogita, J. Read, T. Nishimura, K. Sweatman, S. Suenaga, A.K. Dahle, "Microstructure Control in Sn-0,7mass%Cu Alloys," Materials Transactions, Vol.46 (11), p.2419, (2005).

80. T. Ventura, C.M. Gourlay, K. Nogita, T. Nishimura, M. Rappaz, A.K. Dahle, "The Influence of 0-0.1 wt% Ni on the Microstructure and Fluidity Length of Sn-0.7Cu-xNi," J. Elec. Mat's, Vol.37(1), p.32, (2008).

81. C.M.L. Wu, D.Q. Yu, C.M.T. Law, L. Wang, "Properties of Pb-free Solder Alloys with Rare Earth Element Additions," Mat's Sci. & Eng. R, Vol.44(1), p.1-44, (2004).

82. M.A. Dudek, R.S. Sidhu, N. Chawla, M. Renavikar, "Microstructure and Mechanical Behavior of Novel Rare-Earth Containing Pb-free Solders," J. Elec. Mat's, Vol.35(12), p.2088, (2006).

83. Z. Xia, Z. Chen, Y. Shi, N. Mu, N. Sun, "Effect of Rare Earth Element Additions on the Microstructure and Mechanical Properties of Sn-Ag-Bi Solder," J. Elec. Mat's, Vol.31(6), p.564, (2002).

84. H. Hao, J. Tian, Y.W. Shi, Y.P. Lei, Z.d. Xia, "Properties of Sn3.8Ag0.7Cu Solder Alloy with Trace Rare Earth Element Y," J. Elec. Mat's, Vol.36(7), p.766, (2007).

85. T.H. Chuang, S.F. Yen, "Abnormal Growth of Tin Whiskers in a Sn3Ag0.5Cu0.5Ce Solder Ball Grid Array Package," J. Elec. Mat's, Vol.35(8), p.1621, (2006).

86. S.K.Seo, S.K. Kang, M.G. Cho, D-Y Shih, H.M. Lee, "The Crystal Orientation of -Sn Grains in Sn-Ag and Sn-Cu Solders Affected by their Interfacial Reactions with Cu and Ni(P) Under Bump Metallurgy," J. Elec. Mat's, Vol.38, No.12, p.2461, (2009).

87. P. Lauro, S.K. Kang, W.K. Choi, D.Y. Shih, "Effects of Mechanical Deformation and Annealing on the Microstructure and Hardness of Pb-Free Solders," J. Elec. Mat's, Vol.32, No.12, p1432, (2003).

88. H.-J. Albrecht, A. Juritza, K. Muller, W.H. Muller, J. Sterthaus, J. Villain, A. Vogliano, "Interface Reactions in Microelectronic Solder Joints and Associated Intermetallic Compounds: An Investigation of their Mechanical Properties using Nanoindentation", Proc. 5th Elec. Pack. Tech. Conf. (Piscataway NJ: IEEE), pp. 726-731, (2003).

89. A. Syed, T.S. Kim, S.W. Cha, J. Scanlon, C.G. Ryu, "Effect of Pb-free Alloy Composition on Drop/Impact Reliability of 0.4, 0.5, 0.8mm Pitch Chip Scale Packages with NiAu Pad Finish," Proc. 2007 ECTC, p.951, (2007).

90. M. Amagai, Y. Toyoda, T. Ohnishi, S. Akita, "High Drop Test Reliability: Lead-free Solders," Proc. 2004 ECTC, p.1304, (2004).

91. H. Kim, M. Zhang, C.M. Kumar, D. Suh, P. Liu, D. Kim, M. Xie, Z. Wang, "Improved Drop Reliability Performance with Lead Free Solders of Low Ag Content and Their Failure Modes," Proc. 2007 ECTC, p.962, (2007).

92. P. Elenius, J. Leal, J. Ney, D. Stepniak, S. Yeh, “Recent Advances in Flip Chip Wafer Bumping using Solder Paste Technology”, Proc. of the 49th ECTC, p.260-265, 1999.

93. D. R. Frear, J.W. Jang, J.K. Lin, and C. Zhang, “Pb-free Solders for Flip-Chip Interconnects,” JOM, pp.28-33, (2001).

94. C. Zhang, J.K. Lin, Li Li, “Thermal Fatigue Properties of Pb-free Solders on Cu and NiP Under Bump Metallurgies,” Proc. 51st ECTC, p.463, (2001).

95. S. Terashima, Y. Kariya, T. Hosoi, M. Tanaka, “Effect of Silver Content on Thermal Fatigue Life of Sn-xAg-0.5Cu Flip-Chip Interconnects,” J. Elec. Mat’s, vol.32, no.12, p.1527, (2003).

96. S.K. Kang, P. Lauro, D-Y Shih, D.W. Henderson, T. Gosselin, J. Bartelo, S.R. Cain, C. Goldsmith, K. Puttlitz, T.K. Hwang, “Evaluation of Thermal Fatigue Life and and Failure Mechanism of Sn-Ag-Cu Solder Joints with Reduced Ag Contents,” Proc. 54th ECTC, p.661, (2004).

97. B. Arfaei, Y. Xing, J. Woods, N. Wolcott, P. Tumne, P. Borgesen, E. Cotts, “The Effect of Sn Grain Number and Orientation on the Shear Fatigue Life of SnAgCu Solder Joints,” Proc. 58th ECTC, p.459, (2008).

98. M. Lu, D.-Y. Shih, P. Lauro, C. Goldsmith, and D.W. Henderson, “Effect of Sn Grain Orientation on Electromigration Degradation Mechanism in High Sn-based Pb-free Solders,” Appl. Phys. Lett. 92, 211909 (2008).

99. M. Lu, D-Y Shih, R. Polastre, C. Goldsmith, D.W. Henderson, H. Zhang, M.G. Cho, “Comparison of Electromigration Performance for Pb-free Solders and Surface Finishes with Ni UBM,” Proc. 58th ECTC, p.360, (2008).

100. M Lu, D.-Y. Shih, S. K. Kang, C. Goldsmith, and P. Flaitz,” Effect of Zn Doping on SnAg Solder Microstructure and Electromigration Stability”, J. Appl. Phys. 106, 053509, (2009).

101. S-K Seo, S. K. Kang, D-Y Shih, and H.M. Lee, ”The Evolution of Microstructure and Microhardness of Sn-Ag and Sn-Cu Solders during High Temperature Aging”, Microelectronics Reliability, Vol.49, p.288, (2009).

102. S. K. Seo, S. K. Kang, M. G. Cho, and H. M. Lee, “Electromigration Performance of Pb-free Solder Joints in terms of Solder Composition and Joining Path,” JOM, vol.62, No.7,p.22, July, (2010).

Table 1. Pb-free Solders used in Microelectronic Applications

Composition (wt %)	Liquidus/Solidus (°C)	Applications	Notes
Sn-0.7Cu	227	PTH, Flip chip	Cu dissolution, Wetting, excessive IMCs
Sn-3.5Ag	221	SMT, Flip chip	Cu dissolution, Excessive IMCs, Voids
Sn-3.5Ag-3Bi	208-215	SMT	Cu dissolution Fillet lift, low mp phase
Sn-3.0Ag-0.5Cu (SAC305)	217	SMT, PTH, BGA	Japanese Comm / Consortia Alloy Choice
Sn-3.8Ag-0.7Cu (SAC3807)	217	SMT, PTH, BGA	US Comm Alloy / Europ IDEALS Consortium
Sn-3.9Ag-0.6Cu (SAC3906)	217	SMT, PTH, BGA	NEMI Consortium Alloy
Sn-3.0Ag-0.9Cu (SAC309)	217	SMT, PTH, BGA	US Commercial Alloy

Table 2. US Patents on Pb-free Solders issued during 1988-1999.

US Patents on Pb-Free Solders (1988-999)									
Patent No.	Assignee	Sn (wt %)	Bi	Ag	In	Sb	Cu	Zn	Others
4758407	Harris	87-93		0.1-0.5		4.0-6	3.0-5		Ni
4778733	Engelhard	92-99		0.05-3			0.7-6		
4806309	Willard	90-95	1.0-4	0.1-0.5		3.0-5			
5229070	Motorola	90	1.0-5		5				
5328660	IBM	78	10	2	10				
5344607	IBM	90	2		8				
5352407	Seelig	93-98		1.5-3.5		0.2-2	0.2-2		
5368814	IBM	42	56		2				
5393489	IBM	93	2	3		1	1		
5405577	Seelig	90-99		0.5-3.5		0.2-2	0.1-3		
5410184	Motorola	92-97					3.0-8		
5411703	IBM	94	2			3	1		
5414303	IBM	70-90	2.0-10		8.0-20				
5435968	Touchston	79-97	0-1	0-4			3.0-15		Se
5429689	Ford	80	4.5-14.5		5-14.5				
5455004	Indium Co.	82-90	1.0-5		3.5-6			4.5-6	
5538686	Lucent	> 70	> 10		3.0-10	> 5		6.0-10	
5569433	Lucent	40-60	40-60	0.2-0.5					
5520572	US Army	86-97	0-5	0.3-4.5	0-9.3		0-5		
5527628	Iowa St. U.	89	(5-10)	3.5-7.7			1.0-4	(Si,Sb,Zn	Mg,Ca,RE)
5580520	Indium Co.	71-92		2.0-4	4.0-26				
5658528	Mitsui	90	0.5-1.5	1.0-4	3.0-4				
5698160	Lucent	59-82		2.0-11				16-30	
5718868	Mitsui	90	2.0-3				~0.5	7.0-9	
5733501	Toyota	65-95	0.1-9.5	0.8-5	0.1-9.5	0.1-10			
5730932	IBM	80	12	3	5				
5762866	Lucent	76-98	0.2-6	1.0-6	0.2-6			0.2-6	
5755896	Ford	37-57	37-57		6.0-10				
	Ford	48-58	40-50		2.0-5				
5833921	Ford	43-58	38-52	1.0-2	2	2.0-15	1.0-4		
5837191	Johnson	95		0.6		0.75-2	~0.6		Ni
5843371	Samsung	77-89	6.0-14	3.0-4	2.0-5				
5851482	KIMM	80	1.0-20		0.1-3			0.01-3	Al,Mg,
5863493	Ford	91-97		2.0-5			0-3		Ni
5874043	IBM	70-74		6.5-7.5	12.0-24				
5938862	Delco	84-90		2.5-3.5	7.0-11		0.5-1.5		
5942185	Hitachi	72-87	10.0-23					3.0-5	
5985212	H-Tech	>75			0-6		0.1-9.5		Ga
5993736	Mitsui	91-95	2.0-3	2.0-4				0.5-2	

Table 3. US Patents on Pb-free Solders issued during 2000-2004

US Patents on Pb-Free Solders (2000-2004)									
Patent No	Assignee	Sn (wt %)	Bi	Ag	In	Sb	Cu	Zn	Others
6077477	Matsushita	81-91	5.0-10	3.0-6	0.1-1.0		0.1-2		
6086687	Alpha Fry	>90	0-9.25	0-9.25	0-0.25	0-9.25	0-9.25	0-0.2	Ti
6139979	Murata	92-96				3.0-5	0.7-2.0		Ni
6156132	Fuji Elec	40-70	30-58	0-5		0-5	0-1		Ni, Ge
6176947	H-Tech	balance	0.5-5	2.5-4.5	6.0-12	(0.5-2)	0.5-2.5		
6179935	Fuji Elec	balance		0-4.0		(0-3.5)	0-2.0		Ni, Ge
6180055	Nihon Supr	balance					0.3-07		Ni
6184475	Fujitsu	34-40	46-55	(Ag)	5.0-20	(Sb)		(Zn)	(Ge, Ga, P)
6187114	Matsushita	balance					(0.1-5)		Ni, Pd
6229248	Murata Mfg	balance		1.0-2.0		1.0-3.0	0.5-1.0		
6224690	IBM	balance	1.0-20	1.0-5	(0.5-10)	1.0-10	(0.5-5)	(0.5-5)	Ni,Co
6228322	Sony	balance	0.5-8.0	1.5-6.0			0.1-5.0		La,Ce,Sm,Gd
6231691	Iowa St. U.	balance		3.0-7.7			0.5-4		Fe, Co
6241942	Matsushita	balance	(0.2-6)	0.1-3.5	(0.5-3)		0.1-3	7.0-10	P
	Matsushita	balance	10.0-30	0.05-2				2.0-10	P
6253988	Antaya Tec	30	0.3	4.5	65.0	-0.8	0.5		
6267823	Matsushita	balance	5.0-18	2-3.5	(0.1-1.5		(<0.7)	(<10)	
6296722	Nihon Supr	balance					0.1-2		Ni, Ga
6319461	Nippon Gls	balance	< 10	0.1-6		< 10	0.1-6	0.1-3	Al, Ti
6325279	Matsushita	balance	5.0-10	3.0-6.0	0.1-1.0		0.1-2		
6361626	Fujitsu	balance	3.0-6					3.0-14	Al
6440360	Tokyo First	balance					0.8		Ni
6416883	Ecosolder	balance	20-30	1.0-3.0		< 4.0	< 2.0		
6488888	Matsushita	balance	15-25	0.05-2				2.0-10	
	Matsushita	balance	(0.2-6)	0.1-3.5	(0.5-3)		0.1-3	7.0-10	Ni
6521176	Fujitsu	77-87	10.0-20	2.8-3.1					
6648210	Multicore	balance	1.0-10	< 6		< 5	< 3		
6660226	Murata	> 88		0.5-9			0.5-2.0		Co
	Murata	> 88		3.0-5.0			0.5-1.0		Co
6689488	Taiho Kogyo	balance		1.0-3.5	0.1-2.0		0.1-0.7		Ni Co Fe
6692691	Nihon	balance		3.5-6.0					Ni
	Nihon	balance		3.5-6.0					Ni, P Ga Ge
6703113	Murata	0.1-3.0	> 90	0.1-9.9	0.1-3.0	0.1-3.0	0.1-9/9	0.1-9.9	P, Ge
6805974	IBM	90-95	0.1-0.2	< 2.8			< 1.5		Sb
6824039	IHC	balance		3.0-14					Mg

Table 4. US Patents on Pb-free Solders issued during 2005-2010.

US Patents on Pb-Free Solders (2005-2010)									
Patent No.	Assignee	Sn (wt %)	Bi	Ag	In	Sb	Cu	Zn	Others
6837947	NCK Univ	balance		4.0 >				7.0-10	Al, Ga
6843862	Quantum	88-94		3.5-4.5	2.0-6		0.3-1.0		
6884389	Kabushiki	balance	43-47	0.9-2.2	0.4-0.6		0.4-0.6		Ni Sb Ge
6936219	IKA	balance						7.5-9.0	Mn
6984254	Fujitsu	77-87	10.0-20	2.8-3.1					
	Fujitsu	34-40	46-55		10.0-20				
7022282	Murata	>90.5		0.5-9.0		0.5-5.0			Mn, Cr
7111771	Intel	balance	(Bi)	(Ag)	5.0-15	(Sb)	(Cu)	(Zn)	(Ni,Ge,Pt)
7148426	Hitachi	balance		2.0-5.0			0.01-2.0		P
7172726	Senju	90-98					1.5-8.0		Ni, Co
7175804	Nippon	balance	0.5-6.0					6.0-10	Mg, Al
7175805	Nippon	balance						6.0-10	Mg
7220493	Koa Kabush	balance						30-70	Ni, Al
7224067	Intel		63-67		33-37			(Zn)	Li,Ti,Zr,Re
7250135	MK	>94.79		2.8-4.2	0.2		0.3-0.8		Ge
7273540	Shinryo	balance		2.6-3.4			0.4-0.7		
7282174	Senju	balance	0.5-12			<1.0		5.0-10	AuPtPdFe
7282175	Senju	balance		0.05-5			0.01-0.5		P Ni Co
7335269	Aoki	99 >		0.3-0.4			0.6-0.7		P
7338567	Senju	98 >					0.1-1.5		Ni, P
7410833	IBM	> 90	(Bi)	(Ag)		(Sb)	(Cu)	(Zn)	
7425299	Senju	balance		4.0-6.0			1.0-2.0		
7422721	Murata	90.5					0.5- 2		Pd, Co
7576428	Int Tech Res	0.01-30	30-60		20-70				Ga

Table 5. Melting Temperature and Undercooling of Sn-Ag-Cu Solder Alloys [35].

Alloy Composition (wt %)	Melting Temperatu re (^oC)	Under coolin g (^oC)*
Sn-3.8Ag-0.7Cu	216.9	28.6
Sn-3.4Ag-0.9Cu	217.0	18.0
Sn-3.0Ag-0.9Cu	216.8	21.9
Sn-2.5Ag-0.9Cu	216.8	34.3
Sn-2.0Ag-0.9Cu	216.9	29.3

Table 6. Population of Large Ag_3Sn Plates in Sn-Ag-Cu Solder Alloys Solidified at a Rate of 0.02 C/s [35]

Solder Composition (wt %)	Solder Form	# of Solder Balls with Large Ag_3Sn Plates
Sn-3.8Ag-0.7Cu	BGA balls	76/100
Sn-3.4Ag-0.9Cu	BGA balls	5/100, 10/100
Sn-3.0Ag-0.9Cu	BGA balls	6/100, 3/100
Sn-2.5Ag-0.9Cu	BGA balls	1/100, 0/100
Sn-2.0Ag-0.9Cu	BGA balls	0/100, 0/100
Sn-3.5Ag	Ingot	few
Sn-3.8Ag-0.35Cu	Ingot	many
Sn-3.8Ag-0.7Cu	Ingot	many

Table 7. The Amount of the Undercooling Measured by DSC with Pb-free Solders [29]

Composition (wt %)	Onset Temp (heating) (T_1)	Onset Temp (cooling) (T_2)	ΔT (T_1-T_2)	Peak Temperatures*
Sn-0.9Cu	228.6	199.7	28.9	230.5 (H), 202.0 (C)
Sn-2Ag	228.7	201.5	27.2	230.2(H), 204.5(C)
Sn-1.0Ag-0.9Cu	218.2	192.3	25.9	220.2, 226.0(H), 195.6 (C)
Sn-0.9Cu-0.6Zn	226.8	220.0	6.8	228.7(H) 223.0(C)
Sn-1Ag-0.9Cu-1Zn	217.4	219.2	(-1.8)	219.2, 224.8 (H) 213.0, 219.6 (C)
Sn-0.9Cu-0.3Fe	228.7	208.5	20.2	230.8 (H), 211.9 (C)
Sn-0.9Cu-0.2Co	229.4	224.7	4.7	231.3 (H), 226.3 (C)
Sn-3.0Ag-0.5Cu**	218.7	195.0	23.7	219.7 (H), 195.2 (C)

* DSC 220C, Seiko, heating at 6 $^\circ$C/min, cooling at 6 $^\circ$C/min

** All solder balls are 1.27 mm (50 mil) diameter (~ 8 mg), except for Sn-3.0Ag-0.5Cu, 25 mil diameter (~1 mg).

Table 8. The Minor Alloying Effects on the Undercooling during Sn Solidification [43]

composition (wt %)	ΔT (undercooling)	composition (wt %)	ΔT (undercooling)
pure Sn	**31.2**	Sn-0.2Zn (HCP)	**1.4**
Sn-0.2Pb (FCC)	**34.6**	Sn-0.2Ti (HCP)	**5.4**
Sn-0.2Cu (FCC)	**35.1**	Sn-0.2In (tetragonal)	**22**
Sn-0.2Au (FCC)	**15.5**	Sn-0.2Bi (rhombohedral)	**21.9**
Sn-0.2Cr (BCC)	**21.4**	Sn-0.2Sb (rhombohedral)	**25.5**
Sn-0.2Fe (BCC)	**13.2**	Sn-0.2Se (rhombohedral)	**19.6**
Sn-0.2Mn (BCC)	**22**	Sn-0.2Ga (othorhombic)	**23.5**

Table 9. The Undercooling of Sn-rich Solders with Minor Alloying Elements with a Hexagonal Crystal Structure [43]

Composition (wt %)	ΔT (undercooling)
Sn-0.2Zn	**1.4**
Sn-0.2Co	**6.3**
Sn-0.2Mg	**6.3**
Sn-0.2Ti	**5.4**
Sn-0.2Sc	**4.1**
Sn-0.2Zr	**5.3**

Table 10. Dissolution of Surface Metallization and Intermetallic Growth in Sn-Ag, Sn-Ag-Cu, Sn-Ag-Bi at 250°C [55].

Solder	Surface Metallization	Dissolution Rate (μm/min)	IMC Growth Rate (μm/min)
Sn-3.5%Ag	Cu (4 μm)/Cu	0.20	0.67
	Au/Ni(P)/Cu	0.08	0.49
	Au/Pd/Ni(P)/Cu	0.09	0.42
Sn-3.8%Ag-0.7%Cu	Au/Ni(P)/Cu	0.05	0.47
	Au/Pd/Ni(P)/Cu	0.08	0.55
Sn-3.5%Ag-3.0%Bi	Au/Ni(P)/Cu	0.08	0.70
	Au/Pd/Ni(P)/Cu	0.10	0.67

Table 11. Dissolution and Intermetallic Growth of Ni Metallization (electroless vs electroplated) in Sn-Ag, Sn-Ag-Cu, Sn-Ag-Bi at 250°C [55].

Solder	Surface Metallization	Dissolution Rate (μm/min)	IMC Growth Rate (μm/min)
Sn-3.5%Ag	Au/Ni(P)-(electroless)	0.08	0.49
	Au/Ni-(electroplated)	0.06	0.17
Sn-3.8%Ag-0.7%Cu	Au/Ni(P)-(electroless)	0.05	0.47
	Au/Ni-(electroplated)	0.05	0.29
Sn-3.5%Ag-3.0%Bi	Au/Ni(P)-(electroless)	0.08	0.70
	Au/Ni-(electroplated)	0.05	0.25

Table 12. IMC Growth Kinetics as a Function of Reflow Cycle and Surface Finish at 260C [59].

Module #	Surface Finish (side B)	IMC Thick. (μm)	Surface Finish (side L)	IMC Thick. (μm)	Reflow # at 260 C
1	Cu	5-7	Cu	4-5	2, 1
2	Cu	7-12	Cu	7-9	7, 6
3	Cu	9-17	Cu	9-15	12, 11
4	Au/Ni(P)	3-4	Cu	10-12	2, 1
5	Au/Ni(P)	7-10	Cu	10-11	7, 6
6	Au/Ni(P)	6-10	Cu	8-12	12, 11
7	Au/Ni(P)	3-4	Au/Ni(P)	3-4	2, 1
8	Au/Ni(P)	4-5	Au/Ni(P)	5-6	7, 6
9	Au/Ni(P)	4-6	Au/Ni(P)	4-6	12, 11
10	Au/Pd/Ni(P)	3-5	Cu	5-7	2, 1
11	Au/Pd/Ni(P)	5-8	Cu	5-8	7, 6
12	Au/Pd/Ni(P)	5-12	Cu	8-10	12, 11
13	Au/Pd/Ni(P)	3-5	Au/Pd/Ni(P)	2-5	2, 1
14	Au/Pd/Ni(P)	5-7	Au/Pd/Ni(P)	3-5	7, 6
15	Au/Pd/Ni(P)	4-6	Au/Pd/Ni(P)	3-5	12, 11

Table 13. Thickness of Cu-Sn IMCs and Cu Consumption in Pb-free Solder Joints Annealed for 2000 h at 150C (in µm) [26].

	SAC 305	Zn	Co	Fe	In/Ni	SAC 309	Pb/Sn
Cu Consumption	8.7	5.6	10.9	7.3	11.9	4.9	7.1
Cu3Sn	4.3	0.4	1.5	1.2	1.8	4.2	5.9
Cu6Sn5	7.5	3.4	9.0	9.2	12.2	5.5	5.7

Table 14. Void Propensity Evaluation for Pb-free Solder Joints Annealed at 150°C [26]

Aging at 150 C -1000 hrs	
Solder type	**Average distance between voids (μm)**
SAC305	4
SAC309	2
Aging at 150 C - 2000 hrs	
Solder type	**Average distance between voids (μm)**
SAC305	2.5
SAC+ Zn	570
SAC+Co	3
SAC+ Fe	5
SAC309	2

Fig. 1. Backscattered electron SEM micrograph showing a typical solidified microstructure of Sn-3.8Ag-0.7Cu alloy in a BGA solder ball. Sn dendrite cells are surrounded by Ag3Sn and Cu6Sn5 particulate arrays [15]

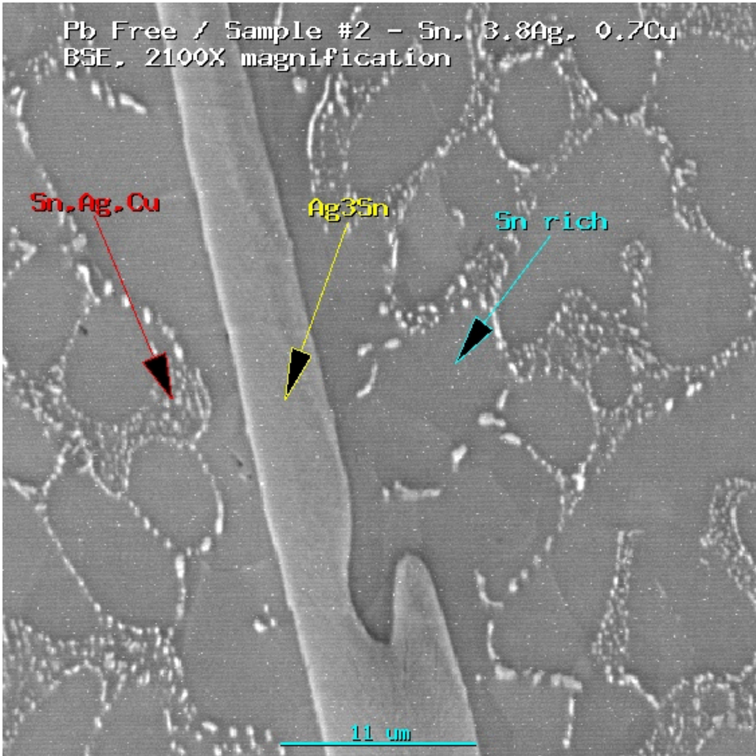

Fig. 2. A BGA solder joint failed by thermomechanical fatigue showing preferred crack propagation along the interface between the Ag3Sn plate (indicated by arrows) and β-Sn phase [13].

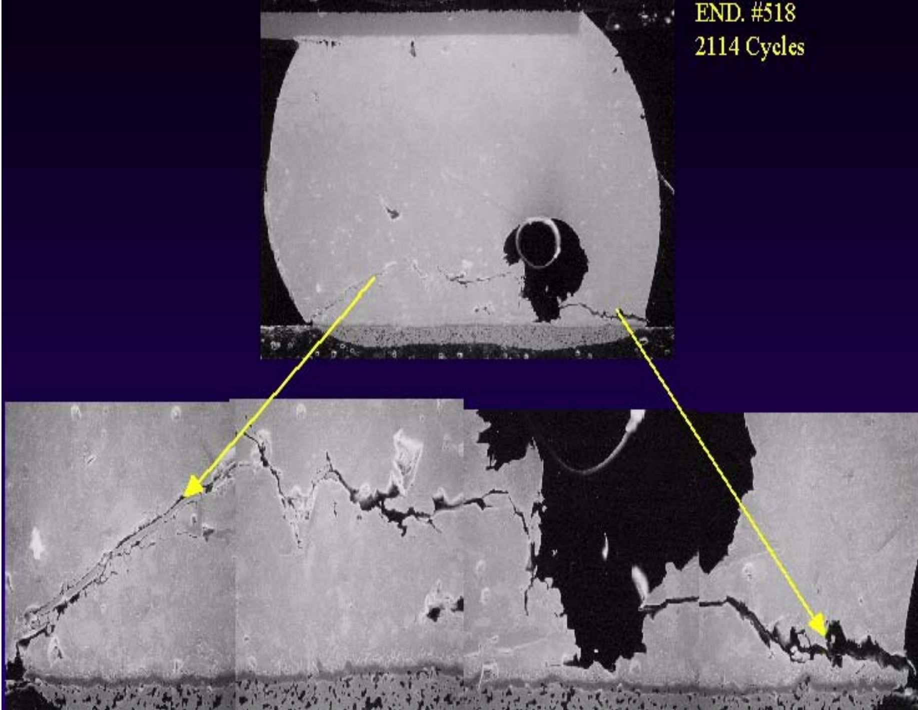

Fig. 3. The intermetallic compounds of Ag3Sn and Cu6Sn5 formed in a flip chip solder joint of Sn-3.8Ag-0.7Cu joined to a Cu subsrate by reflowing twice at 260C (courtesy of T.Y. Lee at UCLA, from [19].

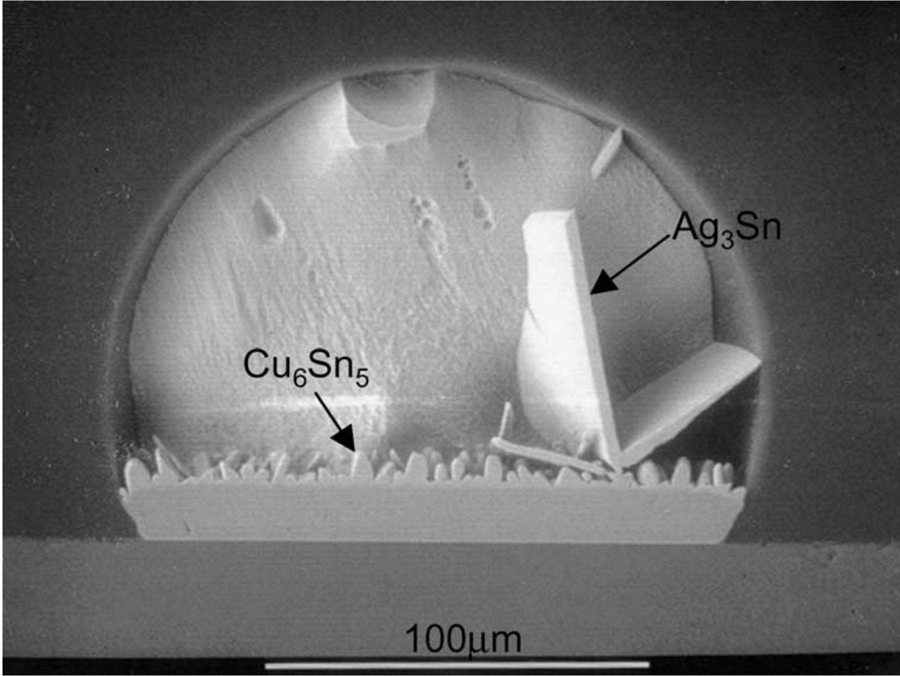

Fig. 4. Electroplated Sn-4.3Ag solder bumps after 20 times reflow. Some solder was etched to reveal Ag_3Sn plates within bumps [37].

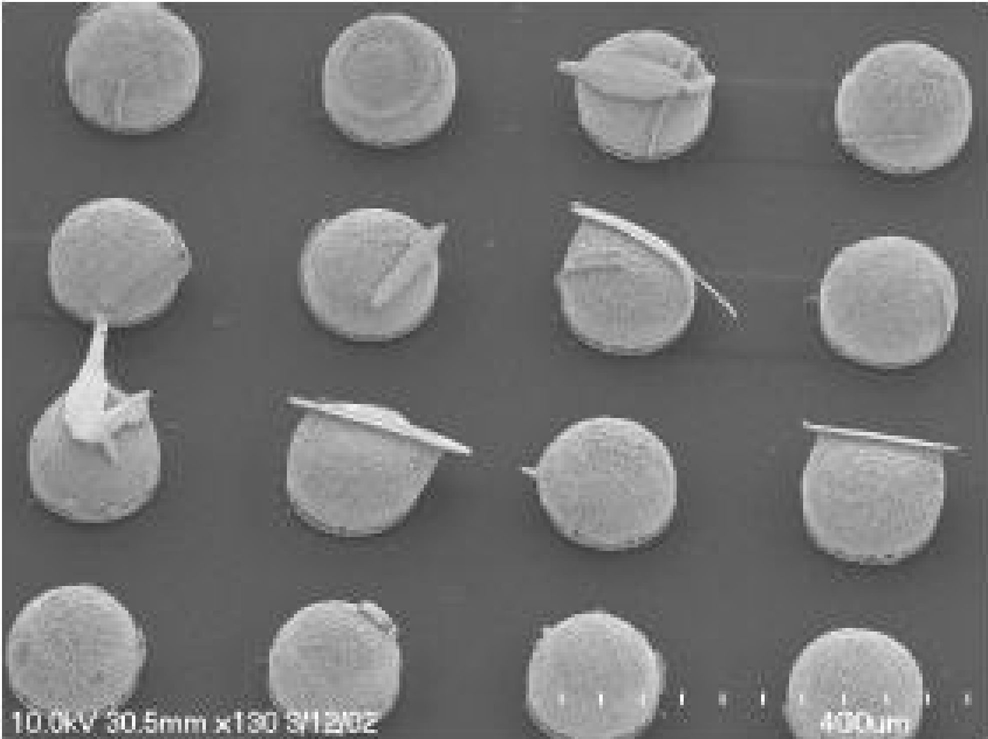

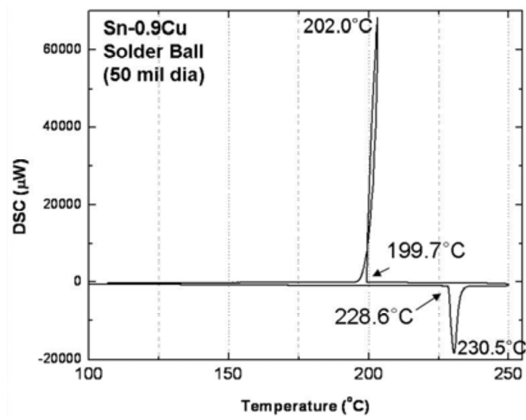

Fig. 5. A typical DSC thermal profile recorded during the heating and cooling cycle of one solder ball of Sn-0.9%Cu (50-mil diameter). The undercooling is estimated to be about 28-29°C depending on either the onset or peak temperatures [29].

Fig. 6

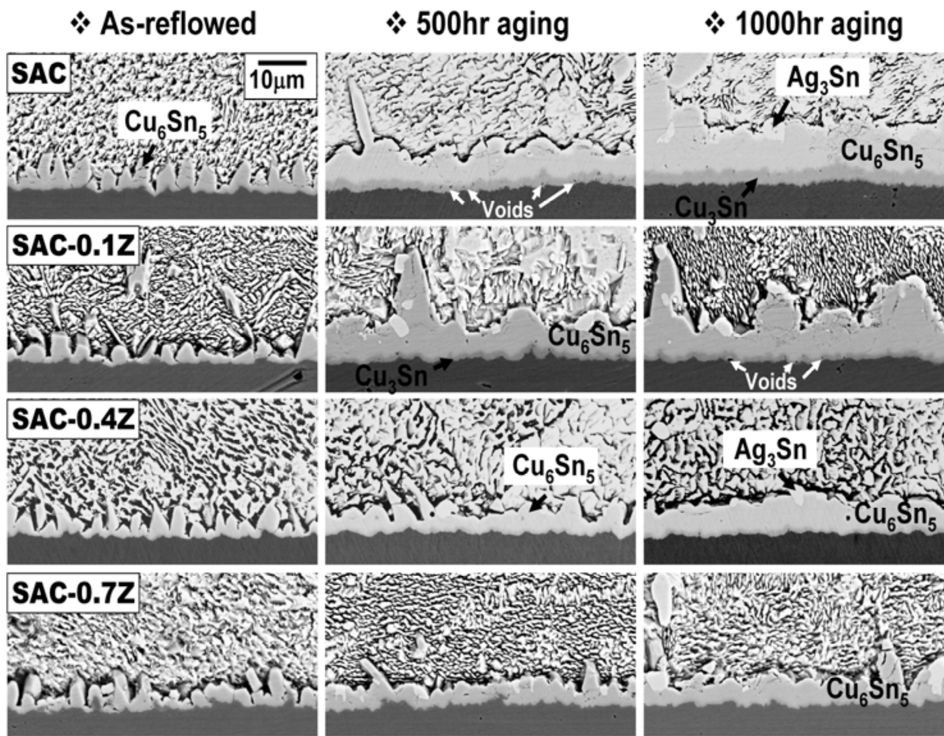

Fig. 6. The cross-section images of Sn-3.8Ag-0.7Cu, Sn-3.8Ag-0.7Cu-0.1Zn, Sn-3.8Ag-0.7Cu-0.4Zn and Sn-3.8Ag-0.7Cu-0.7Zn solders on electroplated Cu after the reflow and aging for 500 h and 1000 h at 150°C [63].

Fig. 7.

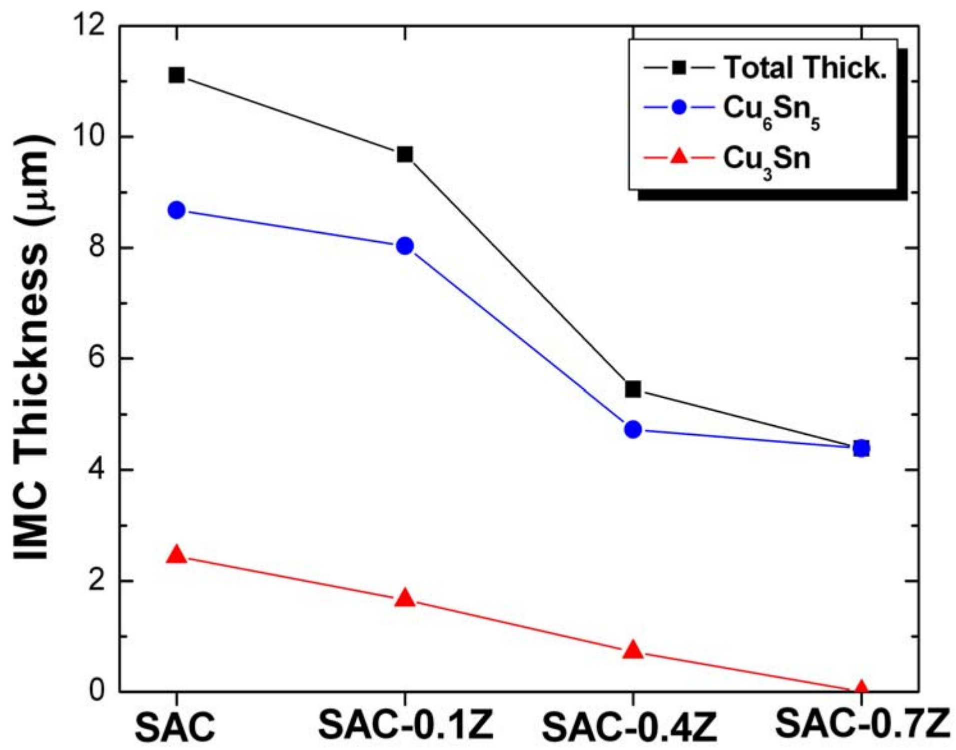

Fig.7. The thickness of each IMC layer plotted as a function of Zn composition in SAC after aging for 1000 h at 150°C on electroplated Cu [63].

Fig.8.

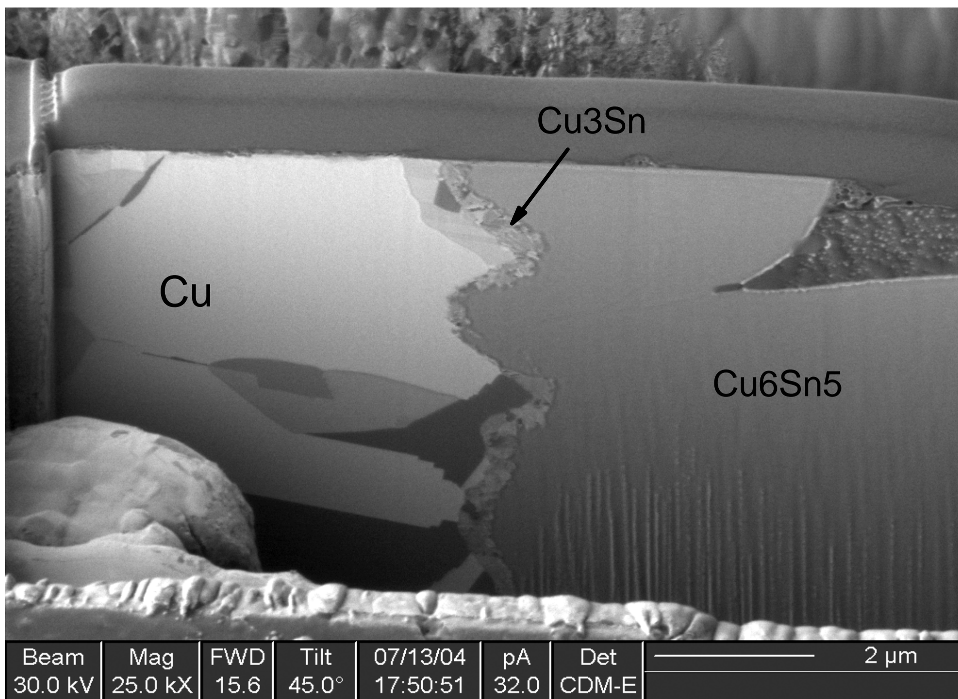

Fig. 8. A secondary electron image of the interfacial region in a SAC+0.7Zn solder joint formed on a Cu pad. The joint was reflowed 10 times with the peak temperature ranging from 235 to 245ºC. The sample was prepared by focused ion beam milling a thin slice perpendicular to the joint interface [25].

Fig. 9.

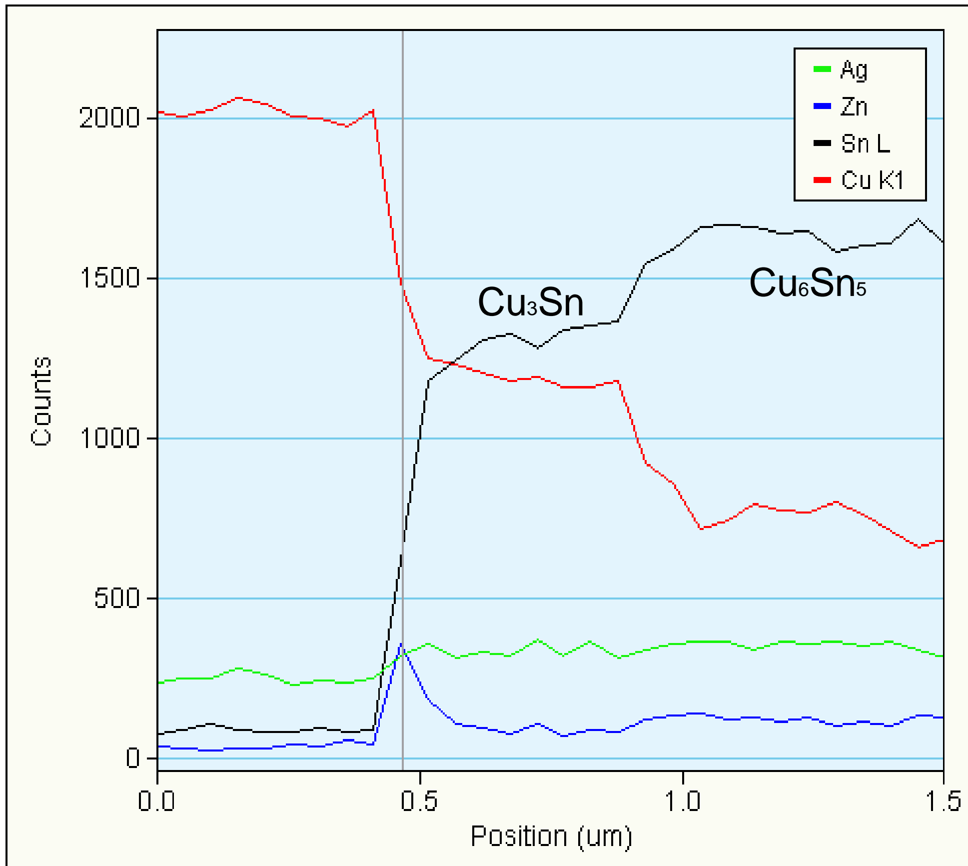

Fig. 9. An example of energy dispersive X-ray (EDX) spectroscopy performed on the sample shown in Fig. 7. The compositional profiles of Cu, Sn, Ag and Zn were plotted along the distance perpendicular to the IMC interfaces [25].

Fig.10. A high-resolution STEM image of the interface between Sn-0.7Cu-0.4Zn and electroplated Cu, aged at 150oC for 1000 h. The micro-analysis results of EDS of the corresponding areas are listed for Cu, Sn and Zn content [43].

TEM Analysis

❖ **STEM image of Sn-0.7Cu-0.4Zn//Cu (aged for 1000 h)**

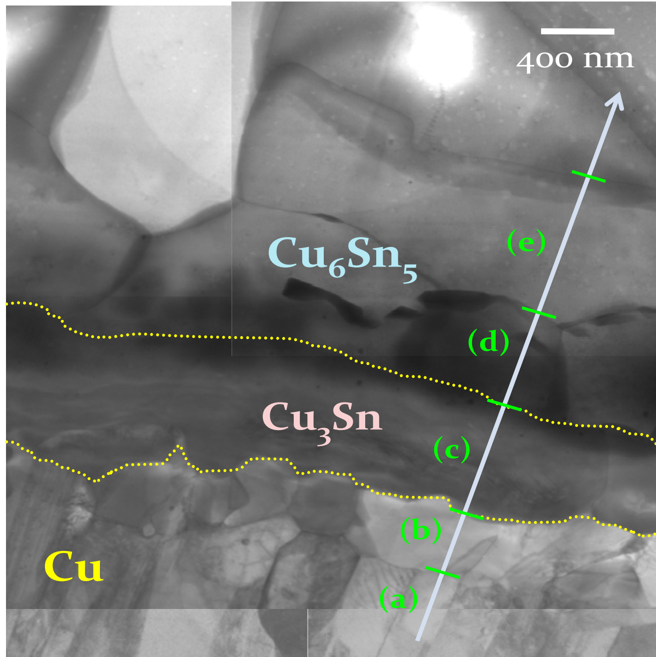

in at% (in wt%)

	Cu_K	Sn_K	Zn_K
(a)	98.3±0.57 (97.2±1.0)	1.2±0.53 (2.2±0.97)	0.54±0.13 (0.55±0.13)
(b)	93.2±2.1 (89.5±3.4)	4.7±1.8 (8.5±3.1)	2.1±0.64 (2.0±0.38)
(c)	78.5±1.2 (66.8±1.1)	20.1±0.90 (32.0±1.2)	1.4±0.8 (1.2±0.69)
(d)	59.6±1.1 (44.5±1.1)	39.2±0.88 (54.7±0.92)	1.2±0.5 (1.0 ±0.44)
(e)	59.1±0.51 (43.8±0.57)	40.1±0.71 (55.6±0.73)	0.81±0.28 (0.62 ±0.21)

✓ 1-2 at% Zn is dissolved in IMC phases (Cu_6Sn_5 and Cu_3Sn) or at the interface of Cu and Cu_3Sn.

Fig. 11

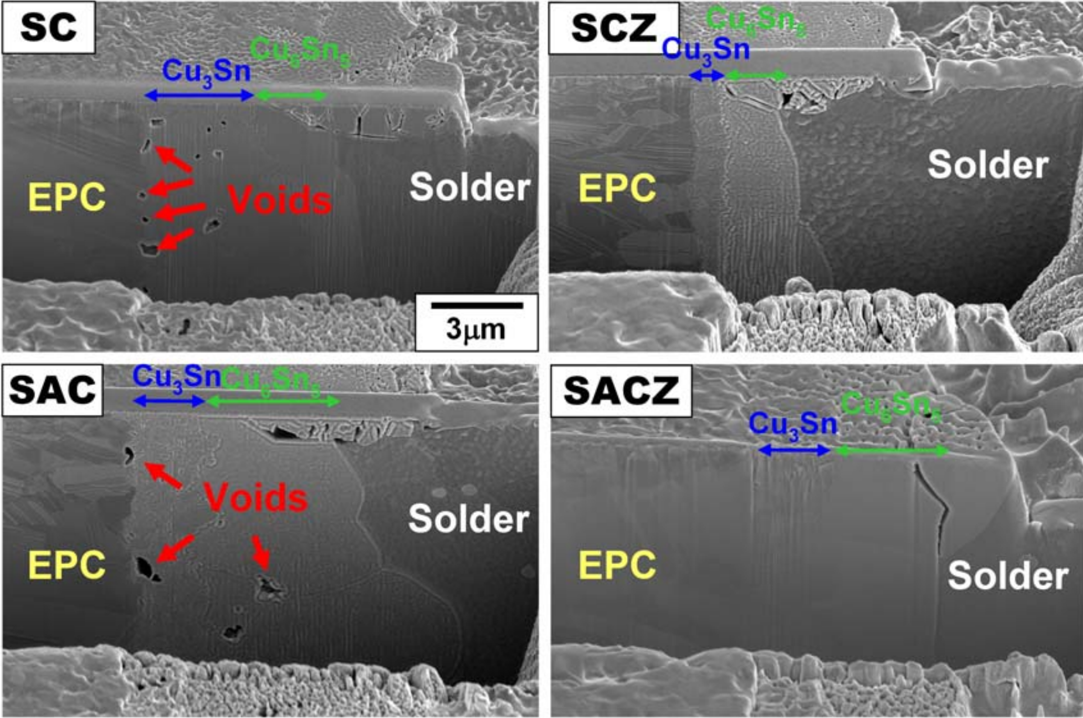

Fig. 11. Secondary electron images of the interface area between each solder and electroplated Cu after aging for 1000 hours at 150°C, which was cut out by the focused ion-beam (FIB) technique [63].

Fig. 12. Cross-polarized images of Sn-Ag solder balls (380 μm diameter) as a function of cooling rate and Ag composition (0, 0.5, 1.0 and 1.8 wt %) [72].

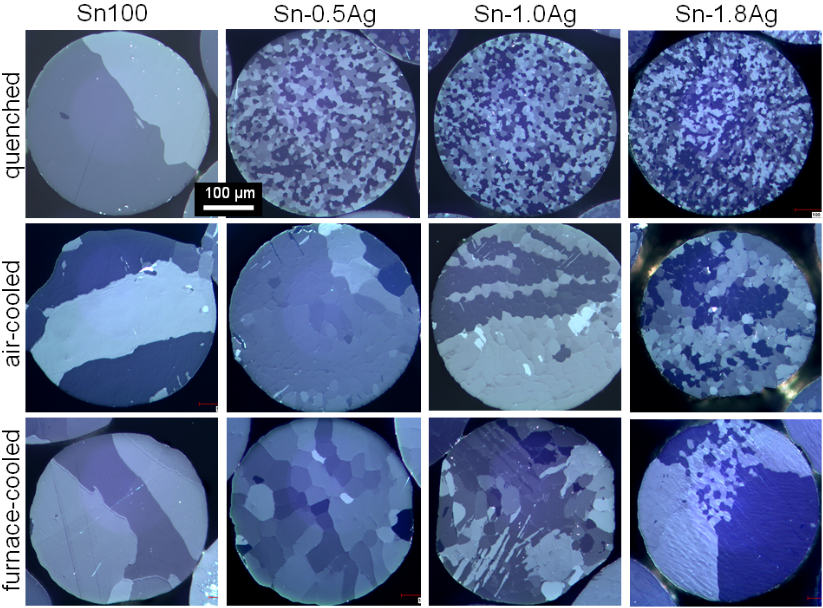

Fig. 13. Cross-polarized images of Sn-Cu solder balls (380 μm diameter) as a function of cooling rate and Cu composition (0.5, 1.0, 1.5 and 2.0 wt %) [72].

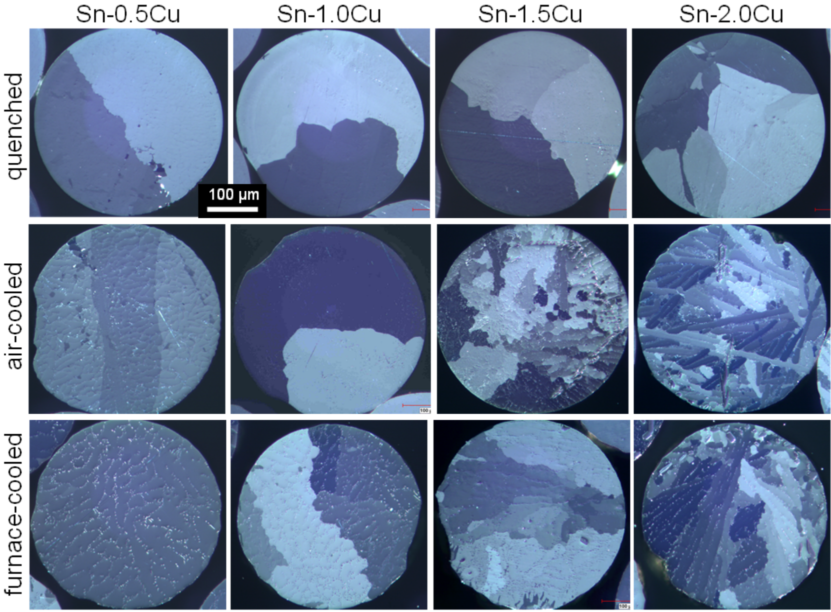

Fig. 13. Cross-polarized images of Sn-Cu solder balls (380 μm diameter) as a function of cooling rate and Cu composition (0.5, 1.0, 1.5 and 2.0 wt %)

Fig. 14.

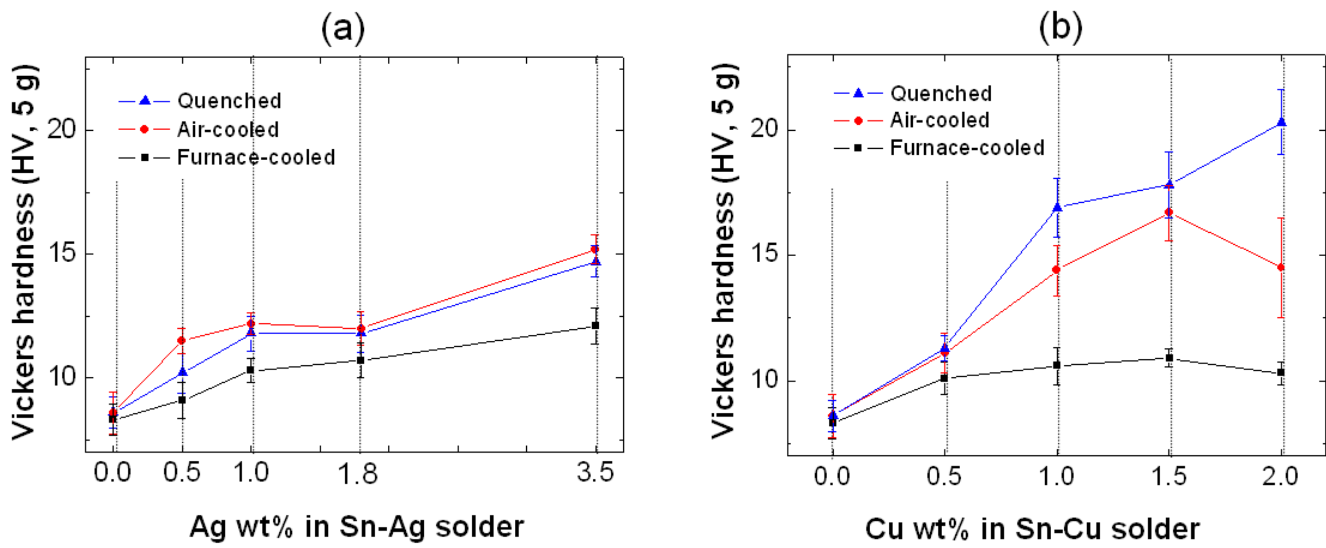

Fig.14. Microhardness variations of (a) Sn-Ag and (b) Sn-Cu solders in terms of solute content and cooling rate [72].

Fig. 15. Cumulative failure probability plot comparing Sn-0.7Cu vs. Sn-1.8Ag. Both solder joints were tested at 90oC at 200 mA [34].

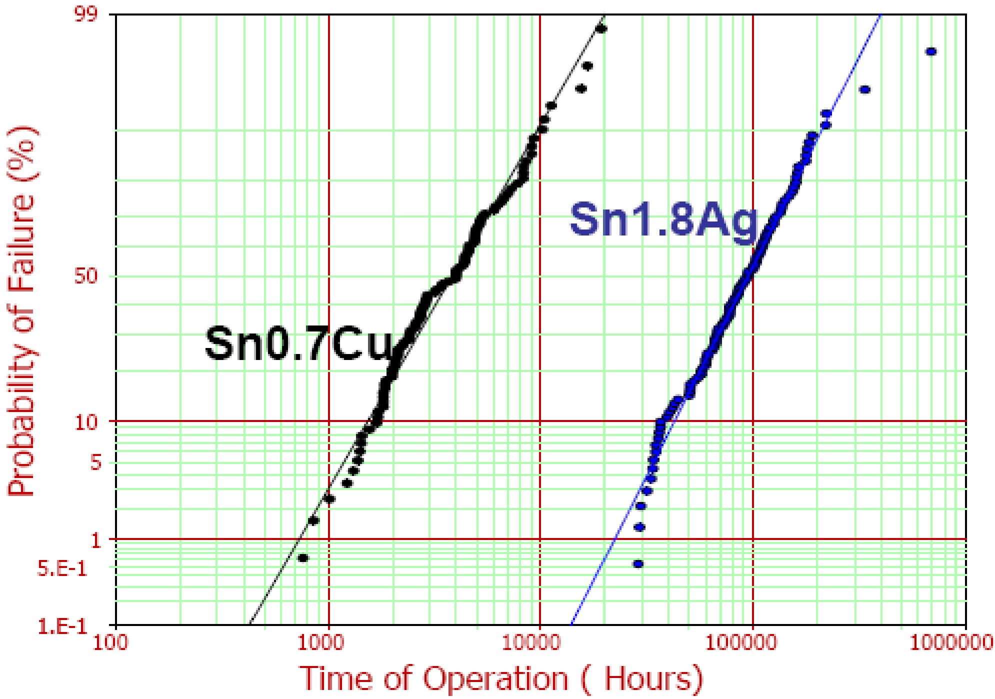

Fig. 16. The lognormal probability plot of the unreliability function for three solder joints; Sn-1.0Ag, Sn-1.8Ag, and Sn-1.0Ag-0.6Zn [34].